

Full length article

Multi-objective optimization of composite stiffened panels for mass and buckling load using PNN-NSGA-III algorithm and TOPSIS method



Tao Zhang^a, Zhao Wei^{a,*}, Liping Wang^a, Zhuo Xue^a, Suian Wang^b, Peiyan Wang^{a,*}, Bowen Qi^c, Zhufeng Yue^a

^a State Key Laboratory of Clean and Efficient Turbomachinery Power Equipment, School of Mechanics, Civil Engineering and Architecture, Northwestern Polytechnical University, Xian, 710072, China

^b School of Mechanical Engineering, Hebei University of Technology, Tianjin, 300131, China

^c Beijing Aerospace Technology Institute, Beijing 100074, China

ARTICLE INFO

Keywords:

Parallel neural network
Composite stiffened panel
Multi-objective optimization
Entropy weight method
TOPSIS technique
NSGA-III

ABSTRACT

A novel multi-objective optimization framework for composite stiffened panels is proposed in this study, leveraging a combination of the Parallel Neural Network (PNN), Non-dominated Sorting Genetic Algorithm-III (NSGA-III), and Technique for Order Preference by Similarity to Ideal Solution (TOPSIS) method. This framework demonstrates high efficiency and accuracy in obtaining the optimal design for intricate optimization challenges. The PNN in this framework, leveraging data-driven methods, addresses the limitations of Classical Laminate Theory (CLT) in constructing optimization surrogate models, such as challenges in parameter range determination, lack of independence, and the necessity for secondary inverse problem solving. In contrast to NSGA-II, NSGA-III which uses reference points and correlation operators achieves more uniform and rich Pareto fronts under stacking sequence constraints. Additionally, to minimize the required effort and expert knowledge in selecting optimal design parameters, this framework incorporates the Entropy Weight Method (EWM) and TOPSIS method. EWM calculates the entropy of optimization objectives from all alternatives in the Pareto front, assigns weights accordingly, and employs TOPSIS to rank the closeness of each alternative to the ideal solution, thereby identifying the optimal design.

1. Introduction

Composite stiffened panels exhibit superior performance in terms of specific stiffness and specific strength, thereby substantially enhancing buckling resistance while minimizing mass requirements. These panels serve as the primary thin-wall structural elements in aerospace and marine applications [1]. The paramount advantage of laminated composite over traditional ones lies in their design flexibility. However, this advantage introduces significant challenges, as achieving diverse structural requirements necessitates altering stacking sequences and discrete variables. Consequently, the plethora of design variable combinations and complex damage mechanisms greatly intensifies design complexities. Thus, there is an urgent need for an efficient and precise optimization methodology to expedite the design process, curtail design expenses, and enhance structural performance [2].

Stiffened panels, as quintessential thin-wall structures, must balance stability and strength, especially under compressive loads where

buckling failure is a significant concern. Therefore, optimizing the buckling load is of utmost importance [3]. However, enhancing buckling properties often comes at the cost of increased structural mass, constraining practical utility. The key challenge, therefore, is to simultaneously maximize compressive buckling loads while minimizing structural mass. The optimization methods that are used to design composite stiffened panels usually derive from laminated plates optimization methods. The optimization challenge for composite stiffened panels is multifaceted, owing to numerous design variables and multi-modal and variable-dimensional optimization problem with unattainable or costly derivatives [4]. The composite optimization problem is non-convex and multi-modal when layer orientations are used as design variables [5,6]. Considering variations in number of piles and the lack of clear positive or negative correlations between single-layer laying angles and optimization objectives. These factors contribute to the highly nonlinear and non-convex nature of composite optimization. The non-convexity results in numerous local optimal solutions, leading

* Corresponding authors.

E-mail addresses: zhaowei@nwpu.edu.cn (Z. Wei), pywang@nwpu.edu.cn (P. Wang).

to the multimodality of the optimization process. Hence, gradient-based optimization methods, like the quadratic lagrangian nonlinear programming algorithm, may or may not reach a local optimum. These algorithms are better suited for optimizing continuous parameters that are amenable to gradient calculations, such as stiffener size, and rib spacing [5]. Evolutionary approaches like Genetic Algorithms (GA) are more suitable for dealing with integer design variables, which have been widely adopted to find the optimal laminate stacking sequences of composite design optimization problems [7–10].

While Finite Element Analysis (FEA) excels in real-time buckling load assessment, its computational demands, particularly for intricate structures or iterative optimization, inflate costs significantly, necessitating swifter, cost-effective alternatives. For this purpose, an efficient design package, VICONOPT, was developed utilizing the accurate stripping method and Wittrick-Williams algorithm [11]. This software is specifically tailored for optimizing laminated composite [12,13]. Furthermore, numerical methods including Isogeometric Analysis (IGA), the Differential Quadrature Method (DQM), the Finite Strip Method (FSM) and surrogate model methodologies including the Response Surface Method (RSM), Radial Basis Function (RBF) and the krygin model were integrated to expedite the optimization process and attain favorable outcomes. Le-Manh et al. proposed an optimal procedure based on GA and NURBS-based finite element IGA for seeking maximum load-carrying capacity of imperfect laminated composite plates [14]. Malekzadeh et al. presented an efficient and accurate differential quadrature (DQ) large amplitude free vibration analysis of laminated composite thin beams on nonlinear elastic foundation [15]. Sadr et al. studied the fundamental frequency optimization of symmetrically laminated composite plates using GA and FSM [16]. Kalnins et al. developed for the design of composite stiffened shells subjected to buckling and post-buckling constraints using GA and RSM [17]. Vijayachandran et al. performed multi-objective optimization to minimize stress concentrations of rectangular plate with an elliptical hole using steered fiberpaths and incorporating realistic manufacturing signatures by GA and RBF [18]. Guo et al. presented a design optimization method for the buckling design of thin-walled variable stiffness composite cylinders using efficient global optimization and kriging model [19].

In recent years, machine learning has become a valuable tool for predicting and evaluating the mechanical properties of composite stiffened panels, owing to its robust nonlinear fitting capabilities and user-friendly operation [20,21]. This is particularly evident in its application to forecasting the buckling properties of composite stiffened panels [22–24]. Current machine learning models compress stacking sequence of different lengths and other features into lamination parameters [25, 26] or their combinations using Classical Laminate Theory(CLT). Although those models showed impressive fitting and generalization performance, they still present certain limitations.

Firstly, since it is based on the Kirchhoff hypothesis, this feature compression leads to information loss [27]. Secondly, these parameters are that they are not independent and cannot be arbitrarily prescribed. The admissible range of lamination parameters are given by solving the geometric relations. Several authors, such as Fukunaga and Vanderplaats [28] and Grenestedt and Gudmundson [29], have suggested necessary conditions for different combinations of lamination parameters, but the complete set of sufficient conditions for all twelve parameters is still unknown [30]. Finally, the lamination parameters strategy requires solving the inverse problem to obtain the corresponding number of plies, thicknesses and fiber orientations, which are suitable for manufacturing. Solving the inverse problem is not easy and the solution is not unique. To address these issues, the Parallel Neural Network (PNN) has been proposed [31], which minimizes information loss through data-driven methods. Its input is consistent with the design parameters, ensuring that the parameters are independent of each other, eliminating the need for solving the inverse problem. Therefore, this paper employs the PNN as the surrogate model.

Existing literature on composite stiffened panel optimization has primarily focused on single-objective optimization. Commonly, the fitness function aims to maximize strength [32], buckling load [33,34], or minimize mass [12,35]. Design parameters typically include stacking sequence, stiffener layout, and ply thickness. However, current surrogate models struggle to accurately capture the mechanical properties of laminated composites under complex optimization variables. This makes it challenging to simultaneously consider stacking sequence, ply thickness, and material properties in the optimization process. Additionally, the current optimization framework for composite stiffened panels lacks a unified approach to address the Pareto front resulting from multi-objective optimization. When the objectives are mechanical properties, such as buckling load or failure load, a unified mechanical indicator—like minimizing the torsional bending coupling coefficient—can serve as a criterion for solution selection [6]. However, if the optimization objectives include non-mechanical indicators, such as mass, volume, or cost, identifying a unified indicator becomes more difficult. L. Marín et al. suggested assigning equal weight to the objective functions as a basis for selecting the optimal panel from the Pareto front [36]. However, this weight allocation lacks a theoretical foundation and may not be applicable to all multi-objective optimization scenarios. Moreover, the traditional multi-objective optimization of composite structures is both labor-intensive and costly, heavily reliant on expert knowledge. Practitioners must possess a deep understanding of the causal relationships between design parameters and multiple objective functions to identify the optimal solution among numerous Pareto solutions. However, such expert knowledge is often scarce, highlighting the need for a method that can objectively and evidence-based identify the best solution from the available Pareto solutions. In conclusion, there is a critical need to establish a more robust surrogate model that can optimize stiffened panels with complex design variables and develop a method to effectively navigate the Pareto front in multi-objective optimization, thus enabling rapid identification of the optimal design solution.

To address the limitations of prior research, this paper introduces a multi-objective optimization framework tailored for composite stiffened panels. This framework encompasses key design parameters including stacking sequences, ply thicknesses, and material properties of both the skin and stiffeners. It pursues multi-objective optimization targeting the maximization of compressive buckling load and the minimization of panel mass. Initially, a comprehensive composite material library is built through extensive reference consultation. Subsequently, a surrogate model is constructed employing the PNN feature extraction method. The optimization process employs the NSGA-III algorithm to concurrently optimize the maximum compressive buckling load and minimum mass of stiffened panels. To enhance the optimization process, a encoding method is introduced for complex design variables, along with a methodology to incorporate stacking sequence design criteria. This approach aims to develop the Pareto front that meets both the objective function and the engineering requirements. Lastly, the obtained Pareto front is subjected to analysis using the EWM and TOPSIS method [37], facilitating the ranking of alternative solutions based on their scores from superior to inferior to get the optimal design.

2. Definition of the multi-objective problem

This section delineates the multi-objective problem by initially presenting the finite element model employed in this study. This model encompasses material properties, dimensions, and boundary conditions, substantiating its accuracy through experimental validation. Subsequently, the variables for multi-objective optimization are defined. Lastly, the objective problem is formulated mathematically.

2.1. Model of the panel: finite element modeling

The dimensions and configuration of the composite stiffened panel

compression specimens are depicted in Fig. 1. As illustrated, a specimen is comprised of skin, stiffeners, and transverse ribs. The skin and stiffeners are crafted from AC531/CCF800H carbon fiber single-layer prepreg composite, boasting a single-layer thickness of 0.14 mm. Meanwhile, the transverse rib is fabricated from aluminum alloy. The overall dimensions of the test specimen measure 541 mm × 780 mm, with stiffener spacing set at 155 mm and rib spacing at 390 mm. The stacking sequences for the skin and stiffeners are detailed in Table 1, while material properties are tabulated in Table 2. Notably, the aluminum alloy boasts an elastic modulus of 71 GPa, a Poisson ratio of 0.33, and a density of 2850 kg/m³.

The compression buckling test is conducted on the test specimen, with the loading diagram depicted in Fig. 2(a). The white numbers in Fig. 2(a) denote the strain gauge identifiers, with corresponding numbers in parentheses indicating the placement of the strain gauges on the rear face of the specimen. Fig. 2(c) showcases the load-strain curves for the region under scrutiny, revealing a pronounced bifurcation at a compressive load of 391 kN, signifying the onset of buckling in the stiffened panels. To discern the buckling modes at this juncture, the trend of the load-strain curve for the positively reacting strain gauge at the same location during buckling is scrutinized. Fig. 2(e) illustrates the buckling mode diagram plotted from the load-strain curve's main observation points. In this study, the finite element model is constructed using ABAQUS, employing S4R shell elements and the mesh seed size is 5 mm, resulting in total element counts of 33,619. Linear eigenvalue buckling analysis is used to obtain the buckling load. The computations are conducted on a device equipped with the 12th Gen Intel Core i7-12,700 CPU and the calculation time is 273 s. Fig. 2(b) delineates the boundary conditions of the finite element model, utilizing the stiffness coupling technique to simulate clamp fixation, while employing the tie contact approach to connect the stiffener and skin. Fig. 2(d) presents a cloud diagram contrasting the finite element model results with the measured buckling loads, demonstrating close agreement with the finite element result of 391.34 kN and the test result of 391 kN, yielding an error margin of merely 0.087 % ($\frac{|FEA_{result} - Test_{result}|}{Test_{result}} \times 100\%$). Moreover, identical buckling modes further corroborate the accuracy of the finite element model, underscoring its reliability. For further insights into the compression buckling test and the finite element model, refer to article [31].

2.2. Definition the design parameters

The design variables for multi-objective optimization of composite stiffened panels are denoted by θ_1 , θ_2 , x_1 , x_2 , x_3 and x_4 , as illustrated in Fig. 3. Here, θ_1 represents the stacking sequence of the skin with θ_1^j indicating the ply angle at the jth layer of the skin. Similarly, θ_2

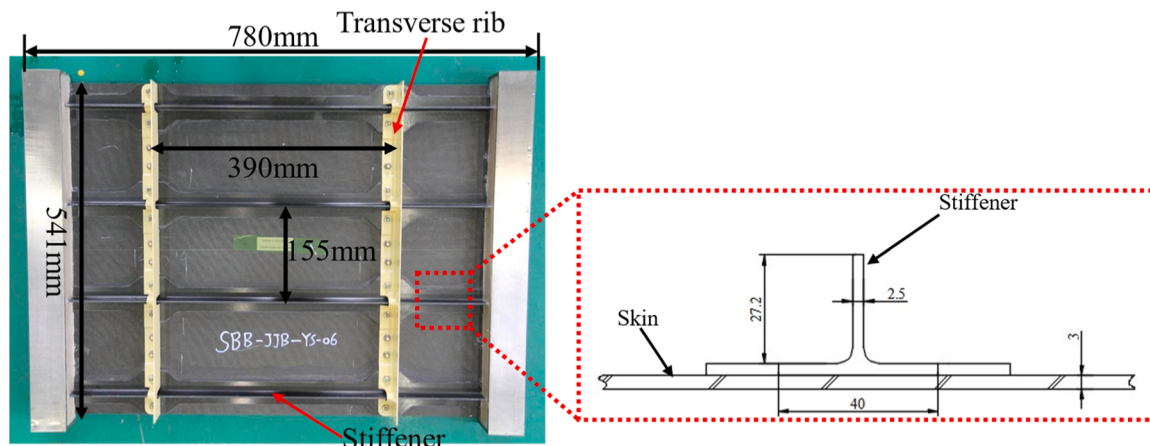


Fig. 1. Schematic diagram of test piece.

Table 1

Lay-up information of specimen.

Material	Lay-up for skin	Lay-up for stiffener
AC631/ CCF800H	[45/-45/0/-45/0/45/0/90/-45/ 0/45/90]s	[45/0/-45/0/90/0/45/0/- 45/0]s

Table 2

Performance parameters of composite materials.

Parameters	Value	Parameter	Value
E_{11}/GPa	155	E_{22}/GPa	8
X_t/MPa	2550	Y_t/MPa	60
X_c/MPa	1440	Y_c/MPa	200
G_{12}/GPa	4	G_{13}/GPa	4
G_{23}/GPa	4	S_{12}/MPa	95
ν_{12}	0.3	$\rho(\text{kg}/\text{m}^3)$	1600

represents the stacking sequence of the stiffener with θ_2^j representing the ply angles at the jth layer of the stiffener. Parameters x_1 and x_2 denote the ply thicknesses of the skin and stiffeners, respectively. And the thickness of each layer is the same. While x_3 and x_4 correspond to the material properties of the skin and stiffeners. There are various types of composite materials available on the market, driven by differences in manufacturing processes and material compositions. As a structural manufacturer, it is often necessary to select from a wide range of composite materials. To simulate this scenario, a composite material library has been developed in this study, drawing from an extensive range of references. Since shell elements are used to model the structural components, the material library exclusively catalogs the lamina properties of the materials employed, as detailed in Appendix A.

2.3. Formulation of the multi-objective optimization problem

In this study, a multi-objective optimization conundrum is delineated, focusing on enhancing the compressive buckling loads of stiffened panels while concurrently minimizing their mass. The design variables pertinent to this optimization challenge are expounded upon herein. Thus, the optimization quandary may be succinctly encapsulated as follows:

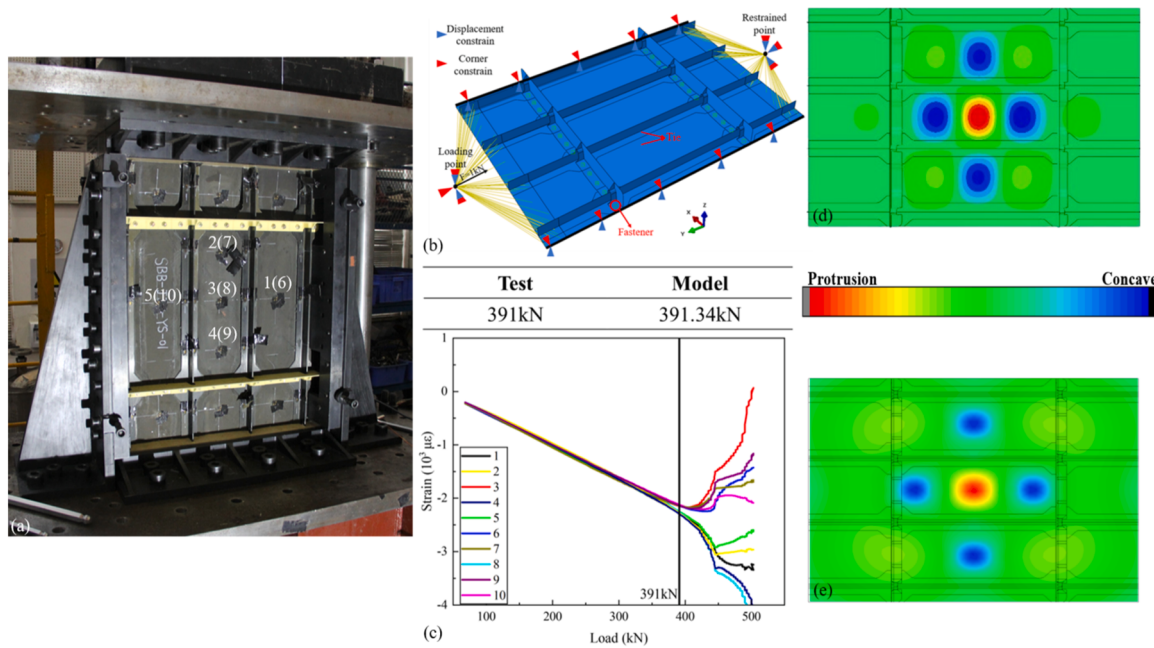


Fig. 2. (a) Test loading diagram (b) boundary constraints (c) strain–load curves (d) buckling mode of finite element analysis (e) buckling mode of test.

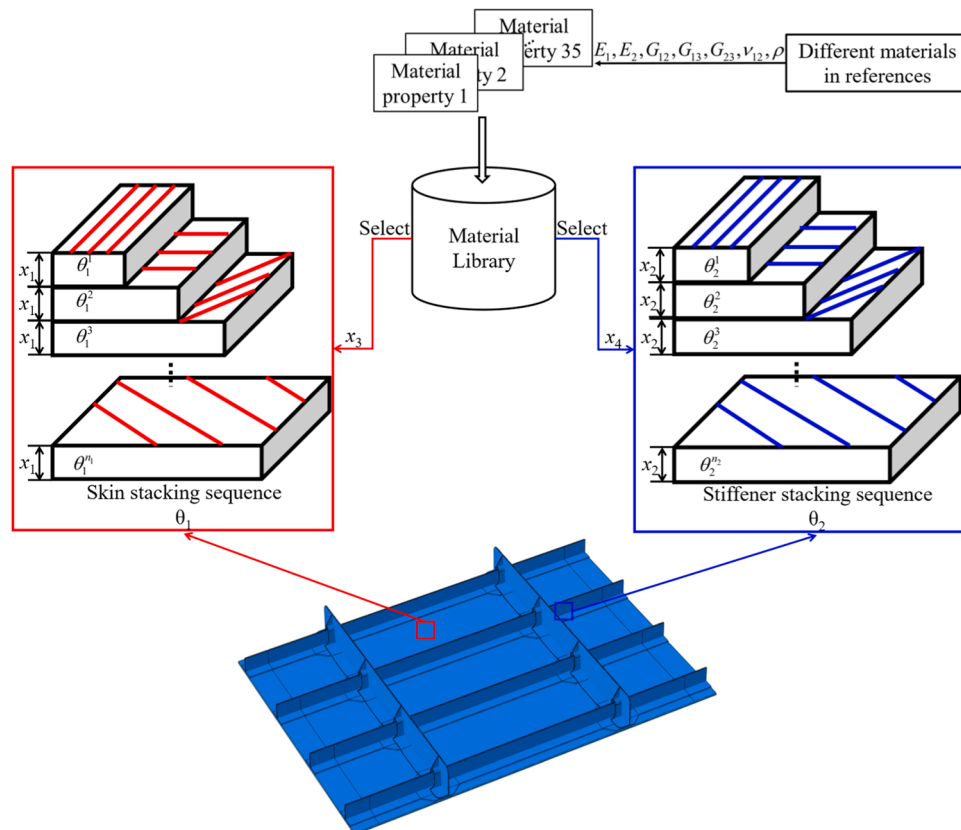


Fig. 3. Design parameters.

$$\begin{aligned}
 & \text{Minimum } \text{Mass}(\theta_1, \theta_2, x_1, x_2, x_3, x_4) \\
 & \text{Maximum } P_b^c(\theta_1, \theta_2, x_1, x_2, x_3, x_4) \\
 & \text{Subject to } \theta_1^i \subseteq \Omega_1, n_1^{\min} \leq i \leq n_1^{\max}, \\
 & \theta_2^j \subseteq \Omega_2, n_2^{\min} \leq j \leq n_2^{\max}, \\
 & x_1^{\min} \leq x_1 \leq x_1^{\max}, \\
 & x_2^{\min} \leq x_2 \leq x_2^{\max}, \\
 & x_3, x_4 \subseteq \Omega_2
 \end{aligned} \tag{1}$$

where, Ω_1 and Ω_2 respectively signify the ply angles of the skin and stringer, characterizing the material property selection space. n_1^{\min} and n_2^{\min} denote the minimum number of layers in the stacking sequence of the skin and stringer. Furthermore, n_1^{\max} and n_2^{\max} represent the maximum number of stacking sequences for the skin and stringer, respectively. x_1^{\min} and x_2^{\min} indicate the minimum ply thickness of the skin and stiffener, while x_1^{\max} and x_2^{\max} denote the maximum ply thickness of the skin and stiffener, respectively.

3. Methodology

The optimization strategy outlined in this article comprises three primary components, detailed comprehensively in Fig. 4. Initially, based on the finite element model established during the preparation phase, a dataset is generated for training and testing the surrogate model using Python scripts. For specific details, please refer to Section 3.1.1. Subsequently, using the Parallel Neural Network (PNN) feature extraction method, a PNN surrogate model is constructed using PYTORCH. The introduction to the PNN feature extraction method is found in Section 3.1, while the detailed steps for constructing the PNN are in Section 3.1.2. The model is then trained and tested. If the model does not converge, convergence can be achieved by adding data points or adjusting the network structure. Firstly, the network learns from data, and if the input variables are complex, the dataset size needs to increase accordingly. Secondly, the network's structure, including its depth, width, activation functions, optimizer, and loss function, significantly affects its fitting and generalization capabilities. Once a robust surrogate model is developed to handle complex design problems involving variable-dimensional and a large number of design variables, the Non-dominated Sorting Genetic Algorithm-III (NSGA-III) algorithm is applied for optimization, as introduced in Section 3.2. Design variables must be encoded, accounting for changes in the number of stacking sequences combined with other design variables, with specific encoding details outlined in Section 3.2.1. Engineering constraints on the stacking

sequence are then introduced, detailed in Section 3.2.2. The selection of crossover and mutation operators follows, with Simulated Binary Crossover (SBX) and Polynomial Mutation (PLM) chosen for this study. The criteria and operator algorithms are described in Section 3.2.3. Finally, the NSGA-III algorithm and PNN surrogate model are used for structural optimization, with the optimization process of NSGA-III explained in Section 3.2.4. Since the algorithm itself is not the primary focus of this paper, only a brief introduction is provided. If the optimization algorithm does not converge, convergence can be achieved by modifying the encoding strategy or adjusting the crossover and mutation operators. The NSGA-III optimization algorithm yields a Pareto front of solutions. In engineering applications, selecting the best solution from this Pareto front can be time-consuming and labor-intensive. Multi-Criteria Decision-Making(MCDM) can streamline the process. This study first applies the Entropy Weighted Method (EWM), which calculates the information entropy of each optimization indicator and objectively assigns weights based on the entropy values. Using these weights, the Technique for Order Preference by Similarity to Ideal Solution (TOPSIS) method identifies the best and worst solutions. By calculating the distances between each solution and both the optimal and worst solutions, the relative closeness of each solution to the ideal is determined, serving as the basis for evaluating quality. Based on these calculations, the Pareto front can be further analyzed to obtain the optimal solution, significantly accelerating the multi-objective optimization process and aiding in the selection of the best design for engineering applications.

3.1. PNN feature extraction method

Previously, surrogate models for stacking sequences with varying number of plies compressed both the stacking sequence features and additional design variables, such as ply thickness, into finite lamination parameters or their combinations based on Classical Laminate Theory (CLT). Using lamination parameters has the big advantage of reducing the number of parameters required to express laminate properties to maximum of 12, regardless of number of layers [38]. However, several limitations persist. Firstly, these lamination parameters are not independent and cannot be assigned arbitrarily. The admissible range of lamination parameters are given by solving the geometric relations. Several authors have suggested necessary conditions for different combinations of lamination parameters, but the complete set of sufficient conditions for all twelve parameters is still unknown [30]. Besides, the lamination parameters strategy requires solving the inverse problem to obtain the corresponding number of plies, thicknesses and fiber

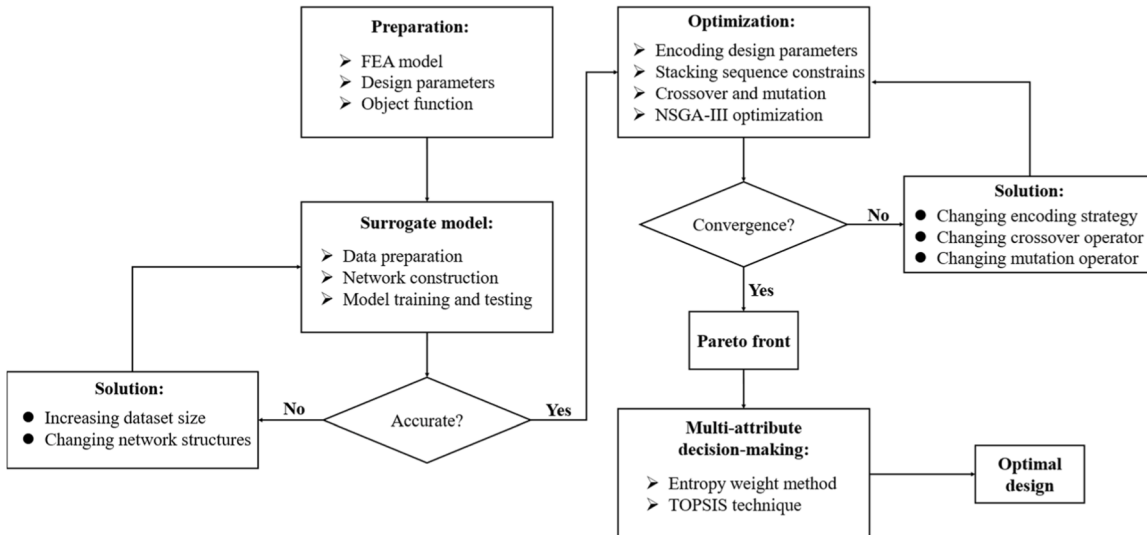


Fig. 4. A flow chart of multi-optimization framework.

orientations, which are suitable for manufacturing. Solving the inverse problem is not easy and the solution is not unique. To overcome these limitations, Parallel Neural Network (PNN) feature extraction methods have been proposed. Extensive research has shown that Recurrent Neural Networks (RNNs) are effective in handling time series problems with variable lengths [39,40], making them suitable for dealing with stacking sequence features, which are composed of ply angles. RNNs can efficiently address stacking sequence problems with varying numbers of layers. However, composite structure optimization involves not only the stacking sequence but also other design variables. Many of design variables are discrete or continuous, which can be effectively handled using the Feedforward Neural Network (FNN). Therefore, this parallel neural network, which processes stacking sequence using a RNN, handles other design variables through a FNN, and fuses the extracted features via vector concatenation, followed by predicting the required mechanical properties through a FNN, is a feasible approach. The PNN minimizes information loss during feature extraction through the data-driven method. Furthermore, its input structure remains consistent with the design variables, ensuring independence and enabling direct determination of their range. As an optimization surrogate model, the PNN also bypasses the need for secondary solving, efficiently providing the optimal design variables. In the previous study, a PNN model was developed to predict the buckling load of stiffened panels with varying skin and stiffener stacking sequences, as well as single-layer thicknesses. The results demonstrated strong fitting and generalization performance [31]. In addition, a novel RNN network structure, Self-attention-based Bidirectional Long Short-Term Memory network (T-Bi-LSTM), was introduced, building on the traditional RNN Bidirectional Long Short-Term Memory network (Bi-LSTM) with an integrated

self-attention mechanism. Self-attention mechanisms are critical in addressing information overload, a common issue in complex networks. Traditionally, attention mechanisms have been incorporated into RNNs to improve their performance [41–43]. Results demonstrate that, compared to Bi-LSTM, T-Bi-LSTM extracts more comprehensive and richer stacking sequence features. For further details on the PNN feature extraction method and related network structures, refer to the relevant research.

3.1.1. Data preparation

In the data preparation phase, the initial step involves determining the parameter range. The ply thicknesses of the skin and stiffener should fall within the range of 0.125 to 0.175 mm, with retention of three significant digits. The ply angles for both the skin and stiffener are chosen from 0°, ±45°, and 90°, employing symmetrical layering. Hence, when utilizing the stacking sequence of the skin and stiffener as input for the network, only half of the input is necessary. The length of half the skin stacking sequence ranges from 8 to 16, while for half of the stiffener stacking sequence, it ranges from 8 to 12. Material property parameters $E_1, E_2, G_{12}, G_{13}, G_{23}$ and ν_{12} are randomly drawn from the material library detailed in Appendix A. Subsequently, leveraging ABAQUS Python for secondary development, a total of 6000 datasets is procured. Subsequent to acquisition, 80 % of this dataset will be allocated as the training dataset for model refinement, while the remaining 20 % will serve as the testing dataset to evaluate the generalization performance of the model.

3.1.2. Network construction

In this paper, the construction of the PNN serves the purpose of

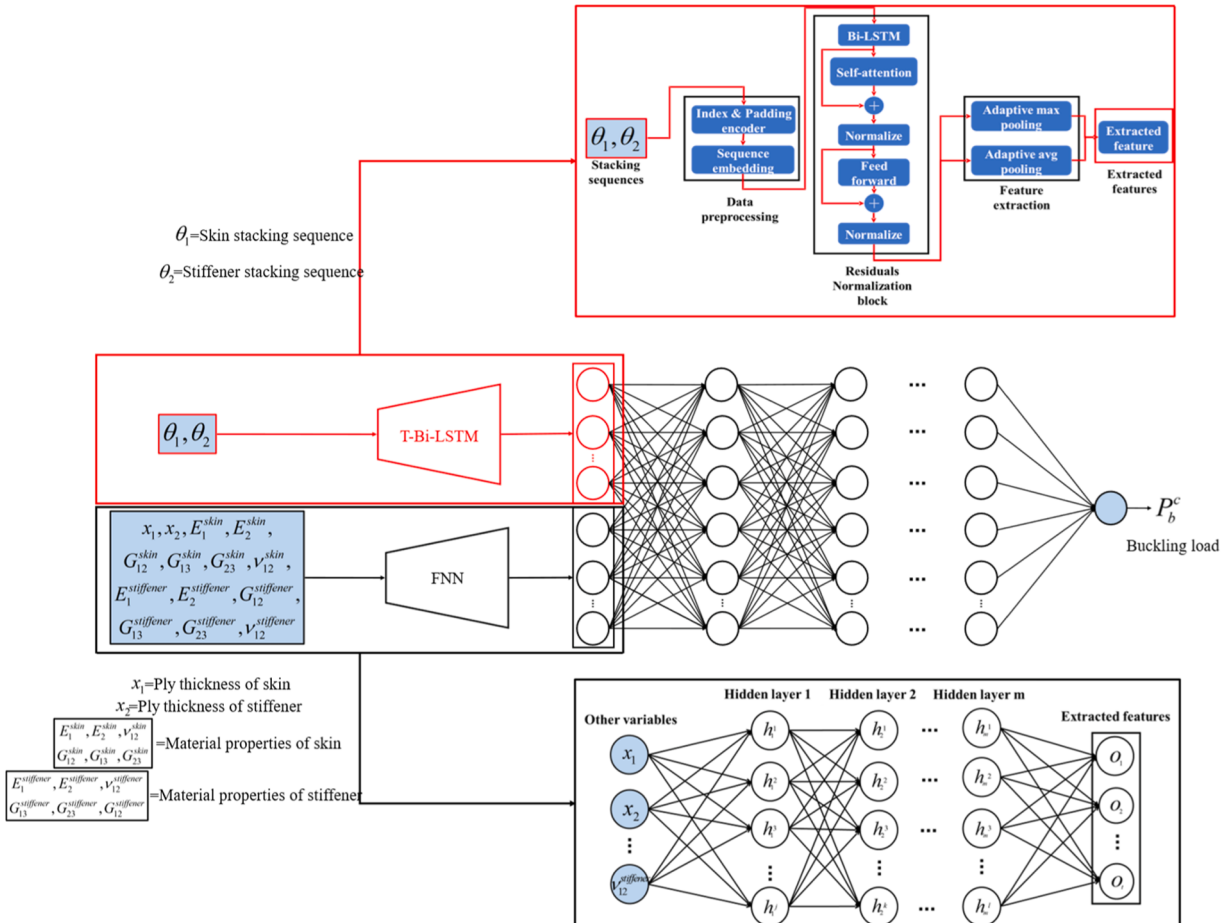


Fig. 5. Network architectures of the PNN.

predicting the compressive buckling loads of composite stiffened panels across varied configurations, including diverse skin and stiffener stacking sequences, ply thicknesses, and material properties. Fig. 5 illustrates the architecture of the PNN, delineated into two primary segments: feature extraction and feature processing.

The initial step is feature extraction. As shown in Fig. 5, the design variables are first divided into two categories: stacking sequence and other design variables. The stacking sequence features are fed into a T-Bi-LSTM network, while the other design variables are processed by a FNN. The T-Bi-LSTM is a novel RNN structure designed to enhance the completeness of feature extraction for stacking sequences. This structure builds on a traditional RNN (Bi-LSTM), and incorporates a self-attention mechanism. Below is a brief introduction to Bi-LSTM and the self-attention mechanism; further details can be found in the relevant literature. The Bi-LSTM neural network consists of two Long Short-Term Memory (LSTM) neural networks with opposing transmission directions: one operating from the front to the back and the other from the back to the front [44]. Consequently, the Bi-LSTM neural network has the capacity to learn from both past and future data. The attention function plays a crucial role in computing the correlation between a query vector and a set of vectors that comprises keys and corresponding values. Weights are assigned to value vectors based on their correlation with the query vector. The ultimate output vector is generated as a linear combination of all the value vectors, as outlined in reference [45]. The structure of T-Bi-LSTM, as illustrated in Fig. 5, consists of three main components: data preprocessing, residual normalization block, and feature extraction. The first step, data preprocessing, involves padding stacking sequences of different lengths into a fixed-length tensor matrix compatible with the PYTORCH deep learning framework. Indexing mitigates the effect of ply angle size on results, while sequence embedding converts discrete ply angles into continuous vectors, expanding the data's dimensionality. This operation improves the richness of data features, as prior research indicates that neural networks perform better when learning from continuous dense data [46]. The residual normalization block is then introduced to accelerate model convergence, speed up training, and improve generalization [47,48]. The integrated self-attention mechanism effectively identifies and processes critical information, enhancing RNN performance [41–43]. The FNN is subsequently used to improve the model's nonlinear fitting ability, boosting its overall learning capacity. Finally, feature extraction is performed using a pooling layer, which, by not requiring parameter training, reduces the risk of overfitting [49]. The combination of max pooling and average pooling enriches feature diversity and completeness. Additionally, the skin and stiffener ply thicknesses along with material variables are incorporated into the FNN other design variables extraction process. Through this data-driven approach, the extraction of both stacking sequences and other design variables is accomplished, enhancing the comprehensiveness and richness of the feature extraction process.

Ultimately, the extracted features undergo processing. For features derived from T-Bi-LSTM and FNN feature extraction, the vectors are amalgamated along feature dimensions through the fusion of vector splicing, a widely adopted technique for extending feature dimensions effectively. Following a sequence of nonlinear transformations and matrix manipulations, the amalgamated features are fed into the FNN feature processor, yielding the compressive buckling loads as output. Notably, both the FNN feature extraction and feature processor in this study utilize the same activation function, SELU, renowned for its self-normalizing property. This characteristic addresses issues such as vanishing or exploding gradients, facilitating faster network convergence and enhancing the model's generalization capability [50]. The formula for SELU is presented as follows (2).

$$SELU(x) = \lambda_1 \begin{cases} x & \text{if } x > 0 \\ ae^x - \alpha & \text{if } x \leq 0 \end{cases} \quad (2)$$

In the formula, λ_1 and α represent the adaptable parameters within the network's learning framework. During network training, input data undergoes sequential transformations to generate output, subsequently necessitating the conversion of the error between network output and the target output into the loss function. Leveraging the backpropagation algorithm, the network's weights and biases are iteratively optimized to minimize this loss function. Within this study, the Adam optimizer is harnessed to minimize the loss function, with the expression of the loss function depicted in Eq. (3). The Adam optimizer exhibits adaptive learning rate adjustments grounded in historical gradient information, facilitating swift convergence with larger initial learning rates, while enabling precise determination of the loss function's minimum with smaller learning rates in later training stages. Additionally, it offers parameter regularization during updates, thereby enhancing network generalization [51]. This article adopts Mean Squared Error (MSE) as the loss function, augmenting the model's generalization capability and mitigating overfitting risks by incorporating an L_2 regularization term into the loss function. The introduction of the L_2 regularization term effectively curbs network size and mitigates overfitting concerns.

$$Loss(y, \hat{y}) = \frac{1}{n} \sum_{i=1}^n (y_i - \hat{y}_i)^2 + \frac{\lambda_2}{2} \| w \|_2 \quad (3)$$

where, y_i represents the true value, \hat{y}_i signifies the predicted value, $\| w \|_2$ denotes the L_2 norm of the parameter vector w , and λ_2 stands for the regularization coefficient. Subsequent to the completion of the model training process, a test dataset is requisite to evaluate the neural network model's performance. In this study, the coefficient of determination (R^2) and the Mean Absolute Percentage Error (MAPE) serve as metrics for assessing the model's generalization prowess, formulated as Eqs. (4) and (5) respectively.

$$R^2 = 1 - \frac{\sum_{i=1}^n (y_i - \hat{y}_i)^2}{\sum_{i=1}^n (y_i - \bar{y}_i)^2} \quad (4)$$

$$MAPE = \frac{100\%}{n} \sum_{i=1}^n \left| \frac{\hat{y}_i - y_i}{y_i} \right| \quad (5)$$

where, \bar{y}_i represents the mean of the actual values.

3.1.3. Model training and testing

In machine learning models, parameters are classified into two categories: model parameters, which are learned from the data, and hyperparameters, which must be predetermined before training and optimized during the process. The wide search space of these parameters significantly impacts the model's outcomes, making the determination of suitable parameter sets a pivotal aspect of model training. In this study, the OPTUNA framework [52] is employed, utilizing simulated annealing to determine parameters. The hyperparameters encompass crucial elements, including the embedding dimension of the stacking sequence following the sequence embedding operation (Embedding size), the dimensions of the T-Bi-LSTM outputs responsible for extracting the skin stacking sequence (Skin hidden size), the dimensions of the T-Bi-LSTM outputs responsible for extracting the stiffener stacking sequence (Stiffener hidden size), the FNN output for extracting other features (Other features hidden size), learning rate of PNN (Learning rate) and loss function regular coefficient (λ_2). In total, the parameters undergo 50 adjustments. Fig. 6 illustrates the parameter adjustment process of the PNN model. The results demonstrate convergence in the parameter adjustments, with the red pentagram denoting the best model.

This article assesses the model's performance from both loss and Mean Absolute Percentage Error (MAPE) perspectives. As model training prioritizes the model's generalization ability, testing loss and testing MAPE serve as indicators to gauge model quality. A lower value of testing loss and testing MAPE indicates a superior model. By

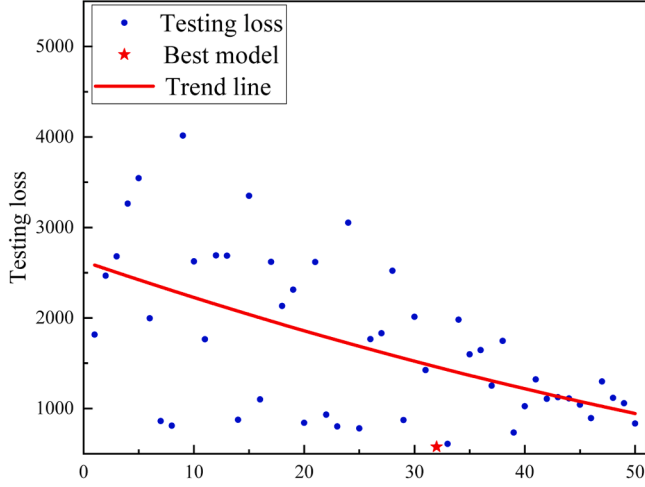


Fig. 6. Parameter adjustment process.

evaluating the neural network models during parameter adjustment, as described earlier, Table 3 presents the parameters of the top ten models along with their corresponding testing loss and testing MAPE values.

3.2. NSGA-III optimization algorithm

In the realm of multi-objective optimization quandaries, conflicts among objectives often arise. For instance, the endeavor to diminish the mass of a stiffened panel might inadvertently diminish its compressive buckling loads as well. Consequently, achieving a solution that concurrently minimizes mass while maximizing compression buckling loads is deemed unattainable. This paper employs the NSGA-III algorithm for the multi-objective structural optimization of composite stiffened panels—a metaheuristic approach extensively employed in addressing multi-objective optimization challenges [53–55].

Non-dominated Sorting Genetic Algorithm (NSGA) represents a multi-objective extension of the genetic algorithm. While the initial version of NSGA is developed based on GA and Pareto frontier principles, it suffers from drawbacks such as high complexity and limited population diversity. Addressing these issues, NSGA-II extends its applicability to a broader range of multi-objective optimization problems [56] by introducing techniques like rapid non-dominated ranking, congestion computation, and elite strategy selection [57]. To enhance both the diversity and uniform distribution of the population, NSGA-III introduces a reference point-based individual selection method, building upon the framework established by NSGA-II [58,59].

3.2.1. Encoding of design parameters

This article encompasses various design variables, including θ_1 , θ_2 , x_1 , x_2 , x_3 and x_4 . Fig. 7 delineates the encoding specifics. Given the diverse nature of these design variables, three encoding methods are employed. Regarding the stacking sequence variables, multiple methods

exist for their encoding in GA optimization problems [60,61]. Here, the concept of empty ply, as proposed in the literature, is utilized to adjust stacking sequence length by removing empty plies [62]. In this scheme, 0, 1, 2, 3, and 4 correspond to empty ply, ply angles 0°, 45°, -45°, and 90°, ensuring uniform chromosome length across individuals and achieving ply length adjustments through empty ply removal. x_1 and x_2 are encoded using real number encoding, while x_3 and v denote the number of selected skin and stiffener materials from the material library, necessitating integer encoding.

3.2.2. Stacking sequence constraints

During the multi-objective optimization process, it's imperative to factor in stacking sequence design guidelines to increase confidence in laminate's long-term structural performance and integrity. Drawing from the insights gleaned from literature [63], the primary considerations revolve around the following ply design requirements: (I) Angle restriction, (II) Symmetry, (III) Balance, (IV) Contiguity, (V) 10 % rule, (VI) Damage tolerance, (VII) Disorientation. Subsequently, a comprehensive delineation of these four design requisites will be provided, along with the methodology for integrating these ply design constraints within the framework of multi-objective optimization. The initial step entails elucidating the specifics of the design requirements:

- (I) Angle restriction: ply angles are typically restricted to 0, ±45 and 90, for which an extensive amount of empirical test data is readily available.
- (II) Symmetry: laminates are restricted to have symmetric stacking sequence to eliminate bending/extension stiffness coupling terms.
- (III) Balance: laminates have the same number of plies of opposite fibre directions (e.g. ±45°) to remove of in-plane shear/extension stiffness couplings.
- (IV) Contiguity: a limit on the number of contiguous plies (this article limits 4 layers) with the same fibre orientation is recommended to prevent crack propagation and ply edge effects.
- (V) 10 % rule: enforcing a minimum amount of stiffness in all directions by having requirements for minimum ply proportions in the 0/90/±45° fibre directions, typically at 10 %, is a common practice to prevent failure from secondary loadings.
- (VI) Damage tolerance: in structures under bending loads, highly loaded plies are protected by placing ±45°plies on the outer surfaces. These plies also increase laminate resistance to impacts, scratches and buckling.
- (VII) Disorientation: the change in orientation between adjacent plies is limited (most commonly to 45°) in order to avoid crack propagation and free-edge delamination.

This study employs optimization techniques focusing on the initial population and penalty functions to regulate stacking sequence design. Initially, given the genetic algorithm's stringent criteria for initial population quality, a methodology inspired by Salih Alan et al. [32] is adopted to enhance the initial population's quality. Subsequently,

Table 3
Result of parameter adjustment.

Embedding size	Skin hidden size	Stiffener hidden size	Other features hidden size	Learning rate	λ_2	Testing loss	Testing MAPE
4096	2048	1024	4096	9.49E-04	1.01E-06	576.7	0.067
4096	1024	2048	4096	9.34E-04	2.87E-06	609.1	0.070
4096	1024	2048	4096	3.08E-04	3.28E-06	733.7	0.078
4096	2048	2048	4096	7.28E-04	2.06E-05	841.6	0.083
4096	1024	2048	4096	2.02E-04	1.93E-06	861.4	0.084
2048	2048	2048	2048	1.39E-03	5.67E-06	872.2	0.087
2048	2048	1024	2048	1.04E-03	1.40E-06	875.7	0.087
4096	1024	2048	4096	1.85E-04	1.41E-06	893.7	0.089
4096	1024	1024	4096	6.95E-04	1.58E-06	932.0	0.090
4096	1024	1024	4096	1.38E-03	3.76E-06	1025.6	0.088

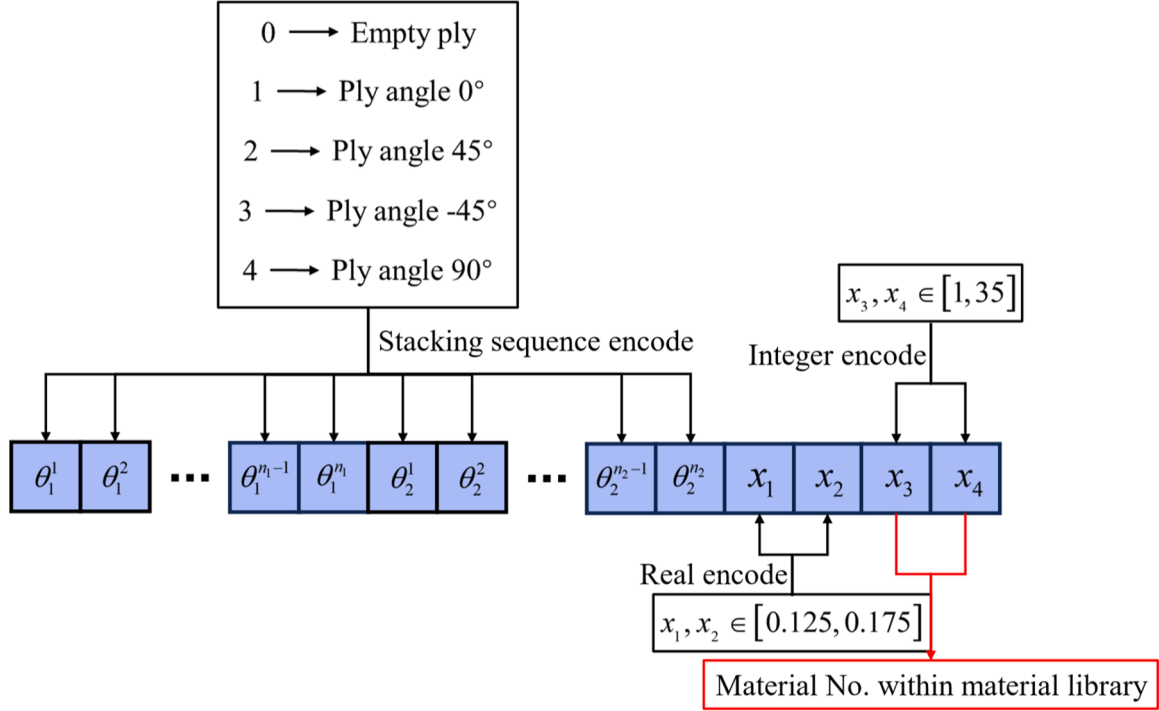


Fig. 7. Encoding of the design parameters.

individuals failing to meet the aforementioned design specifications incur augmented penalty terms. A greater penalty is deducted from their maximal objective function, while an amplified penalty is appended to their minimal objective function, thereby ensuring the elimination of non-compliant individuals throughout the optimization process.

3.2.3. Crossover and mutation

The crossover operator stands as a pivotal element within evolutionary algorithms [64]. Among these, the Simulated Binary Crossover (SBX) emerges as a widely embraced choice, originally rooted in real-coded genetic algorithms. SBX orchestrates variable recombination between two parent generations, yielding two offspring via a probability distribution centered around the parental generation. This mechanism ensures offspring proximity to the parental traits, with a propensity for favoring offspring resembling their parents. Demonstrated efficacy across numerous continuous optimization challenges [65–67] underscores the suitability of SBX for this paper's objectives. The SBX crossover operator operates as follows: given two n-dimensional parent individuals, denoted as $P^1 = (x_1^1, x_2^1, \dots, x_n^1)$ and $P^2 = (x_1^2, x_2^2, \dots, x_n^2)$, and their respective offspring C_i^1 and C_i^2 , new individuals are generated via the crossover process, as delineated by formula (6), thereby producing the subsequent generation of individuals.

$$SBX(P^1, P^2) = \begin{cases} C_i^1 = 0.5[(1-\beta)x_i^1 + (1+\beta)x_i^2] \\ C_i^2 = 0.5[(1+\beta)x_i^1 + (1-\beta)x_i^2] \end{cases} \quad (6)$$

where, the distribution factor β is determined by formula (7).

$$\beta = \begin{cases} (2\mu)^{\frac{1}{\eta_c+1}} & \mu \leq 0.5 \\ [2(1-\mu)]^{\frac{1}{\eta_c+1}} & others \end{cases} \quad (7)$$

where, η_c represents a user-defined parameter, wherein a higher η_c value signifies offspring closely resembling the parents, while a lower value accentuates disparities between the offspring and parental traits. μ denotes a random number within the interval $[0, 1]$.

Mutation operators exert a pivotal influence on control optimization,

thereby significantly impacting the efficacy of single or multi-objective evolutionary algorithms. Hence, the careful selection of mutation operators holds paramount importance in enhancing the optimization algorithm's performance [68]. Past research underscored the superiority of Polynomial Mutation (PLM) over random mutation, non-uniform mutation, and power mutation within real-coded genetic algorithms [69]. Building upon these findings, this paper integrates the efficacious PLM operator into multi-objective optimization endeavors. The PLM operator is delineated by the following formula.

$$PLM(x_i) = x_i + (\max(x_i) - \min(x_i))\delta_m, i = 1, 2, \dots, n \quad (8)$$

$$\delta_m = \begin{cases} (2r)^{\frac{1}{\eta_m+1}} - 1 & r \leq 0.5 \\ 1 - [2(1-r)]^{\frac{1}{\eta_m+1}} & others \end{cases} \quad (9)$$

where, η_m denotes the mutation constant, and r represents a random number within the range of $[0, 1]$.

3.2.4. Optimization procedure

NSGA-III operates within the same framework as NSGA-II. However, it differs in its approach to solution selection. While NSGA-II employs the congestion distance as a solution competition scheme, NSGA-III utilizes a series of reference point-based methods to identify optimal solutions for many-objective optimization problems. These methods encompass determining reference points, self-adapting normalization of population members, association operations, and niche reservation operations.

The optimization process, exemplified in Fig. 8, initiates by generating the initial population following the range and coding method delineated in Fig. 7, along with the population initialization approach detailed in Section 3.2.2. Subsequently, it constructs a set of uniformly distributed reference points within the target space to effectively guide the search towards a well-distributed Pareto front. Next, leveraging the PNN trained in Section 3.1, it acquires the compressive buckling loads corresponding to each individual. The mass corresponding to each individual is then computed using the material density sourced from the

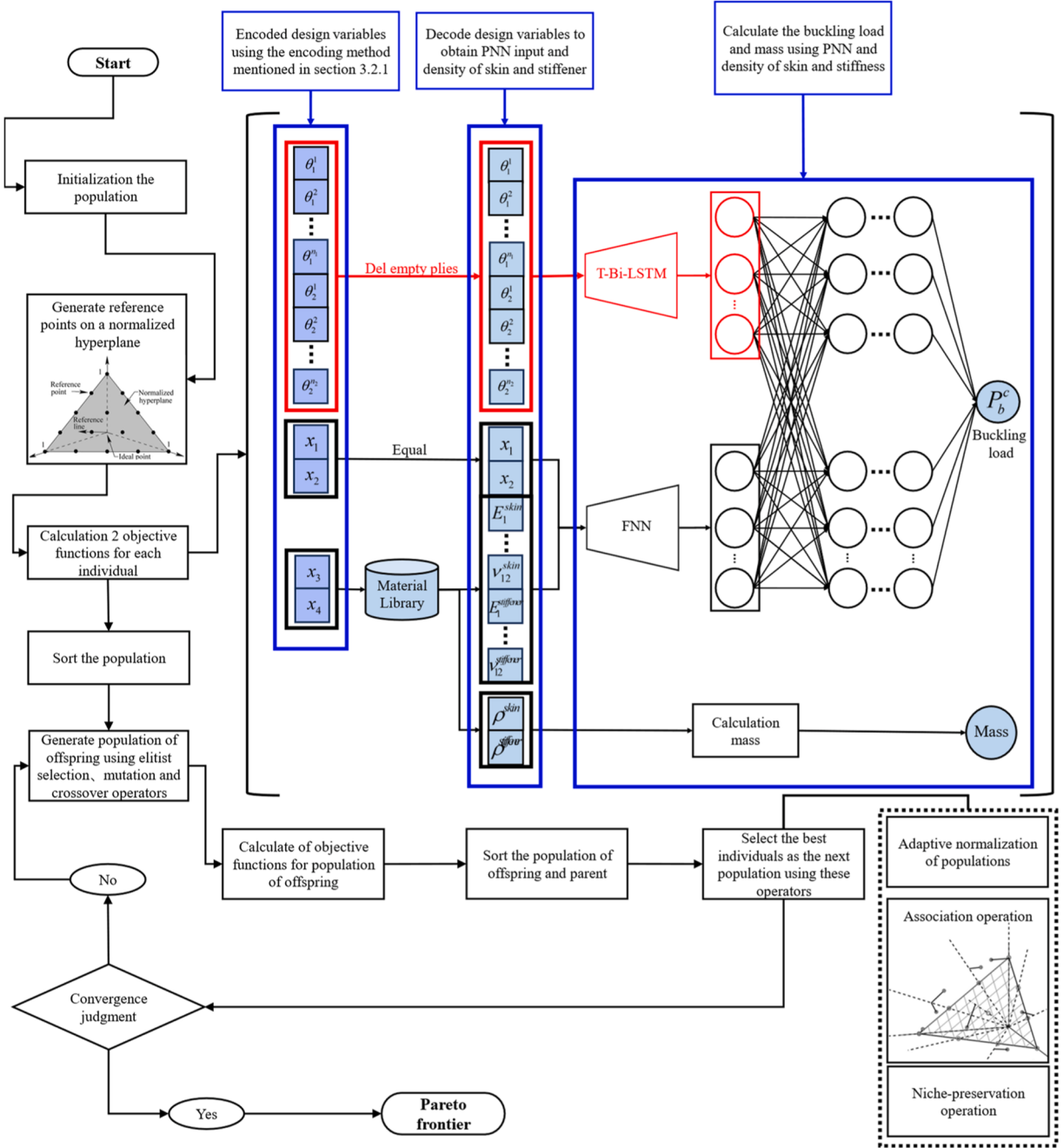


Fig. 8. Optimization procedure.

library. This is succeeded by sorting the non-dominance relationship among individuals in the population based on the aforementioned three target value magnitudes. Utilizing the non-dominated rank, a binary tournament selects parents (P_t) for the population, from which children (Q_t) are generated employing the SBX crossover operator and the PLM mutation operator. Subsequently, the objective function value of the child is computed, and it is amalgamated with the parent to constitute the population (R_t), which is subsequently sorted non-dominantly. Ultimately, the individuals in R_t necessitate screening. Initially, adaptive normalization operations are conducted for R_t , followed by associating each individual with its reference point of minimum vertical distance in the target space. At this juncture, the individuals associated with and around each reference point form a clustering category, regarded as a niche. To ensure solution diversity, it is imperative to guarantee an adequate number of individuals within each niche, a process termed

niche preservation operation. By executing the above steps, the individuals in R_t are retained through filtration. Should the termination criteria be met (e.g., reaching the maximum number of iterations), the current non-dominated solution is returned as the final Pareto frontier; otherwise, the current population undergoes selection, crossover, and mutation anew. Detailed insights into reference point generation, reference point association, non-dominated ordering, and reference point-based niche retention policies can be found in relevant literature [55, 70].

3.3. Multi-attribute decision-making

NSGA-III furnishes the decision maker with a set of Pareto optimal solutions, termed Pareto front. Consequently, decision makers often face the task of selecting an optimal solution from this frontier, constituting a

multi-attribute decision-making (MADM) conundrum. Technique for Order Preference by Similarity to Ideal Solution (TOPSIS), recognized as a potent solution to MCDM challenges, has found widespread application across logistics [71], manufacturing [72,73], marketing [74], and engineering [75]. The efficacy of the TOPSIS method in resolving MCDM issues underscores its adoption for tackling the Pareto front derived from NSGA-III, facilitating the acquisition of the optimal solution.

3.3.1. Entropy weight method

Prior to utilizing the TOPSIS method for assessing the merits and demerits of different choices, it becomes imperative to allocate weights to each objective parameter. In previous studies, when the objective function encompasses all mechanical performance indicators, criteria such as minimizing the bending-torsion coupling coefficient can be utilized for design selection [6]. However, when optimizing the objective function involves non-mechanical performance indicators like mass, volume, or cost, it becomes challenging to identify a unified metric for solution selection. L. Marín et al. suggested assigning equal weight to the objective functions to select the optimal wall panel from the Pareto front [36]. However, this weight allocation lacks a theoretical foundation and is not universally applicable to all multi-objective optimization tasks. The Entropy Weight Method (EWM) offers an objective weighting approach, determining indicator weights based on the information content of each value. Indicators with lower entropy exhibit greater variation, providing more information; thus, their contribution to the comprehensive evaluation warrants a higher weight. This method accounts for the correlations and differences between indicators in the multi-objective optimization design process, allowing for objective weight assignment based on entropy. The calculation of indicator weights through EWM entails the following steps:

The original matrix R representing m evaluation objectives based on n independent indicators is as follows:

$$R = (r_{ij})_{n \times m} = \begin{bmatrix} r_{11} & r_{12} & \cdots & r_{1m} \\ r_{21} & r_{22} & \cdots & r_{2m} \\ \vdots & \vdots & \ddots & \vdots \\ r_{n1} & r_{n2} & \cdots & r_{nm} \end{bmatrix}_{n \times m} \quad (10)$$

where, r_{ij} signifies the evaluated value of the j^{th} objective of the i^{th} indicator. To enable comparison, the raw data necessitates consolidation into dimensionless values. In this study, the extremal method is employed for normalization. The normalized matrix E is illustrated in formula (11), with the extremal method formula delineated in formula (12).

$$E = (e_{ij})_{n \times m} = \begin{bmatrix} e_{11} & e_{12} & \cdots & e_{1m} \\ e_{21} & e_{22} & \cdots & e_{2m} \\ \vdots & \vdots & \ddots & \vdots \\ e_{n1} & e_{n2} & \cdots & e_{nm} \end{bmatrix}_{n \times m} \quad (11)$$

$$e_{ij} = \frac{r_{ij} - \min(r_i)}{\max(r_i) - \min(r_i)}, i = 1, 2, \dots, n; j = 1, 2, \dots, m \quad (12)$$

Subsequently, the information entropy value l_i is computed:

$$l_i = \frac{\sum_{j=1}^m q_{ij} \ln q_{ij}}{\ln m}, i = 1, 2, \dots, n \quad (13)$$

where q_{ij} is calculated as follows:

$$q_{ij} = \frac{e_{ij}}{\sum_{j=1}^m e_{ij}} \quad (14)$$

Finally, the weight value w_i of the i index is obtained:

$$w_i = \frac{(1 - l_i)}{\sum_{i=1}^n (1 - l_i)} \quad (15)$$

3.3.2. Technique for order preference by similarity to ideal solution method

Traditional multi-objective optimization of composite structures is labor-intensive and costly, which largely relies on expert knowledge. It requires practitioners to have a deep understanding of the causal relationship between design parameters and multiple objective functions in order to select the best solution from a large number of Pareto solutions. However, this expert knowledge is very rare, so the Technique for Order Preference by Similarity to Ideal Solution (TOPSIS) method is adopted is needed to objectively and evidence-based obtain the best solution from Pareto solutions. TOPSIS excels at ranking and selecting multiple alternatives amidst the presence of numerous evaluation indicators. The core principle of this method involves first identifying the positive and negative ideal solutions for each indicator. The positive ideal solution represents the best possible outcome, where all indicators achieve their optimal values among the candidate solutions, while the negative ideal solution denotes the least favorable outcome. Subsequently, the Euclidean distance between each solution and both the positive and negative ideal solutions is calculated, allowing for the determination of each solution's proximity to the optimal solution. This proximity serves as a criterion for evaluating the quality of the solutions. The TOPSIS method is constructed through the following steps:

The normalization matrix E is derived by employing the identical normalization scheme as outlined in Eq. (12) of Section 3.3.1, while the weight re-normalization matrix H is structured by acquiring the weight values for each index utilizing the EWM approach.

$$H = (h_{ij})_{n \times m} = \begin{bmatrix} h_{11} & h_{12} & \cdots & h_{1m} \\ h_{21} & h_{22} & \cdots & h_{2m} \\ \vdots & \vdots & \ddots & \vdots \\ h_{n1} & h_{n2} & \cdots & h_{nm} \end{bmatrix}_{n \times m} \quad (16)$$

$$h_{ij} = e_{ij} \times w_i \quad (17)$$

Next, the ideal point (α^+) and the non-ideal point (α^-) are calculated:

$$\alpha_i^+ = \max(h_{ij}) \quad (18)$$

$$\alpha_i^- = \min(h_{ij}) \quad (19)$$

It's crucial to highlight that for the mass parameters in this study, given the objective of minimizing mass, the calculation of the ideal and non-ideal points concerning the mass parameters should be reversed from Eqs. (18) and (19). Subsequently, the similarity between each alternative and the ideal and non-ideal points is determined, commonly elucidated using the Euclidean distance. This distance is computed from the ideal and non-ideal points as follows:

$$d_j^+ = \sqrt{\sum_{i=1}^n (\alpha_i^+ - h_{ij})^2} \quad (20)$$

$$d_j^- = \sqrt{\sum_{i=1}^n (\alpha_i^- - h_{ij})^2} \quad (21)$$

After obtaining the similarity, the proximity coefficient (T_j) for each alternative needs to be calculated as follows:

$$T_j = \frac{d_j^-}{d_j^+ + d_j^-} \quad (22)$$

Sorting the alternatives by the size of T_j and selecting the option with the largest T_j as the optimal choice.

4. Result and discussion

The result of this paper is primarily categorized into three sections. Firstly, the performance of the PNN in predicting buckling loads is showcased, highlighting its accuracy. Secondly, by employing the NSGA-III and NSGA-II algorithms, the Pareto front resulting from the multi-objective optimization of stiffened panels is revealed, emphasizing the NSGA-III algorithm's superiority in addressing boundary issues in stacking sequence design. Lastly, a demonstration of employing the TOPSIS method to resolve the Pareto front is provided.

4.1. Prediction of buckling load

A total of 6000 data are generated, with unsolvable data eliminated (the maximum eigenvalue order is limited to 5 to optimize computation time). Consequently, if no positive eigenvalues are identified, the results of this calculation are deemed unusable), resulting in 5662 data. Among these, 1132 data are designated for testing. To assess the neural network's performance on the untrained testing dataset, in Fig. 9, the discrepancy between FEM buckling loads and those predicted by the PNN is depicted. The red dots denote PNN predictions, evenly distributed on either side of the black line where true values align with predicted values. The R^2 stands at 0.968, with the MSE of 500.827. The MAPE for testing samples averages 6.7 %, with only 18 % of all samples exhibiting errors exceeding 10 %. In summary, the PNN model developed in this study accurately forecasts the buckling loads of stiffened panels under complex optimization variables, demonstrating suitable generalization properties.

4.2. Optimization results

For this multi-objective optimization, composite stiffened panels undergo optimization using the NSGA-III and NSGA-II algorithms, aiming to minimize mass while maximizing buckling loads, respectively. The algorithms are executed on the 12th Gen Intel Core i7-12,700 CPU. The population size is set at 500, with the crossover parameter η_c at 30 and the mutation parameter η_m at 20. In this study, the criterion that the iteration ceases once the number of Pareto frontier solutions equals the population value is established. Fig. 10(a) and (b) depict the optimization outcomes achieved using the NSGA-II and NSGA-III algorithms, respectively. The blue spheres in the diagram represent the Pareto front derived from this optimization, where each point signifies an optimal design. Analysis of Fig. 10 reveals a pronounced inverse relationship between buckling loads and mass: as mass decreases, buckling loads

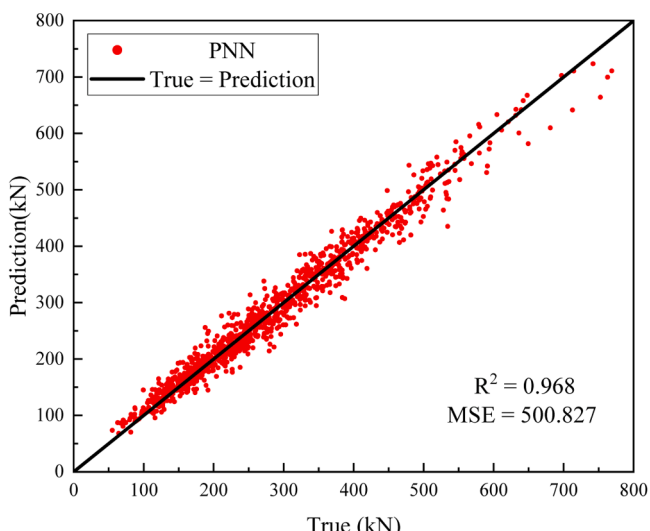


Fig. 9. PNN predictive performance.

decrease, and vice versa. This observation underscores a significant conflict between the two objectives. The green triangle denotes the original design employed in the experiment detailed in Section 2, while the red-framed area indicates a superior design characterized by higher buckling loads and reduced structural mass. Comparing the results of Fig. 10(a) and (b), it is evident that the Pareto front generated by NSGA-II optimization is uneven, discontinuous, and lacks richness. This front features a significant number of repeated solutions and fewer optimal designs. This lack of continuity and abundance stems from many solutions failing to adhere to stacking sequence design specifications and consequently being discarded. The NSGA-II algorithm struggles to sustain solution diversity solely through non-dominated ordering, leading to a concentration of Pareto solutions around certain points and a proliferation of duplicate solutions. Consequently, the performance of the NSGA-II algorithm falls short when confronted with complex boundaries. In contrast, the NSGA-III algorithm leverages a suite of reference point-based techniques to enhance the richness and uniformity of Pareto solutions. This enables the generation of sufficiently diverse solutions within the boundary constraints typical of complex industrial designs. Notably, the Pareto solutions yielded by NSGA-III showcase a plethora of superior designs. However, the process of sorting and verifying these designs individually demands significant time, resources and expert knowledge. Hence, there arises a pressing need for a methodology capable of assigning varied target weights in multi-objective optimization challenges for composite materials, facilitating the sorting of resulting Pareto frontier designs from optimal to suboptimal.

The iterative processes of the NSGA-III algorithm and the NSGA-II algorithm are subjected to further analysis. In Fig. 11(a) and (b), the quantity and distribution of the Pareto solutions generated by both algorithms throughout the iterative process are depicted, respectively. Fig. 11(a) illustrates that while the NSGA-II algorithm achieves rapid convergence, its Pareto solution distribution is discontinuous and uneven. Analyzing the trend of its Pareto front reveals a limited search range, resulting in solutions clustering near the initial distribution points and preventing the formation of a continuous front. This leads to low population richness and significant population assimilation. Despite mutation operators that partially enhance diversity, the constraints of layer design make it challenging to maintain solution variety through non-dominated sorting alone. In contrast, Fig. 11(b) shows that the Pareto front produced by NSGA-III optimization is continuous and uniform. The overall optimization process exhibits initial oscillation followed by rapid convergence. The oscillation stems from the elimination of prior Pareto solutions, indicating that NSGA-III explores a broader solution space beyond initial distribution points. The subsequent distribution is refined based on the framework established after elimination, suggesting that the reference point-based selection method of NSGA-III effectively filters out inferior solutions in early iterations, ensuring a consistent and rich Pareto front. In summary, under complex design boundary constraints, the NSGA-III algorithm demonstrates enhanced capability in searching for high-quality Pareto solutions and maintaining population diversity compared to NSGA-II.

The buckling analysis solution time utilizing FEA and PNN stands at 118 s and 1×10^{-4} s, respectively. Remarkably, the buckling analysis time employing PNN represents a mere 0.00008 % of that required by FEA, marking a significant reduction in computational expenditure. Given that 49,000 buckling evaluations were conducted for this GA optimization, PNN facilitated a total time savings of 1606 h, averaging 32.78 h per iteration. Notably, the mentioned PNN solution time in this discourse excludes training time, as the PNN model can be deployed infinitely once training concludes.

4.3. Optimal design

Following the algorithmic process described earlier, a set of Pareto solutions is derived, delineating an improved design range from the original benchmark design. Consequently, the optimal design must be

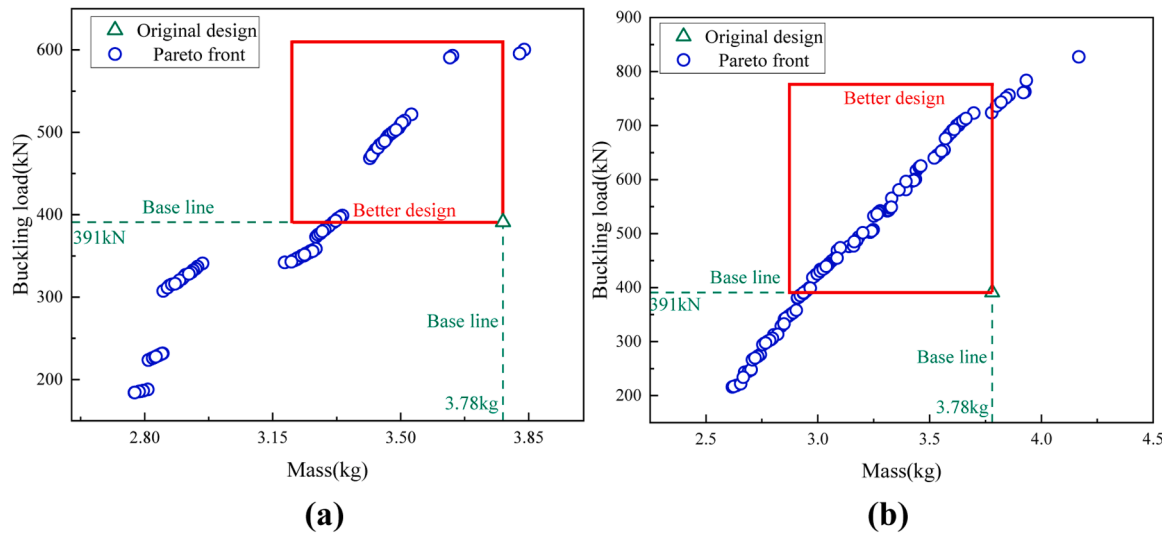


Fig. 10. Pareto fronts of (a) NSGA-II and (b) NSGA-III algorithm.

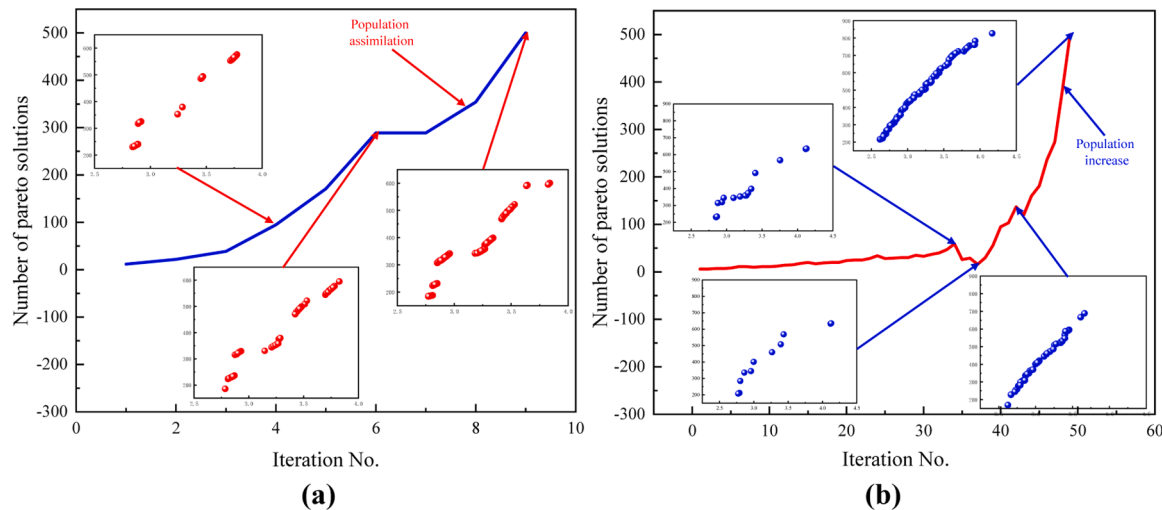


Fig. 11. Iterative processes of (a) NSGA-II and (b) NSGA-III algorithms.

discerned from within these refined solutions, constituting a MCDM challenge. This paper employs the TOPSIS method to address the aforementioned Pareto solutions, with Fig. 10 showcasing the resultant solutions. Initially, the weight coefficients for mass and buckling loads are determined using the EWM. It is noteworthy that any value of 0 encountered after normalization through the EWM could render subsequent logarithmic calculations impossible if left untreated. Thus, this article addresses this issue by reassigning any normalized 0 value to 1E-8. The column depicted in the figure illustrates a solution with weight coefficients of 0.4986 for mass and 0.5014 for the buckling load. Subsequently, the TOPSIS method is employed to calculate the score for each solution. As outlined in Section 3.3.1, the score is normalized using the Extreme Value Method. The final Pareto solution, indicated by a score of 1, represents the optimal design, depicted by the red pentagon in Fig. 12. This article stipulates that a score exceeding 0.9 denotes a favorable design, as indicated by the black sphere in Fig. 12. Table 4 presents the top three design parameters ranked by their scores, along with a comparison of buckling loads to mass with the original design. Notably, all top three designs utilize Material Library No 16 for the stiffeners and Material Library No 30 for the skin. Both the skin and stiffeners stacking sequences are identical, comprising [45/0₂/-45/90/45/0₃/-45/0]_s and [45/0₃/-45₂/90/45/0]_s, respectively. The primary

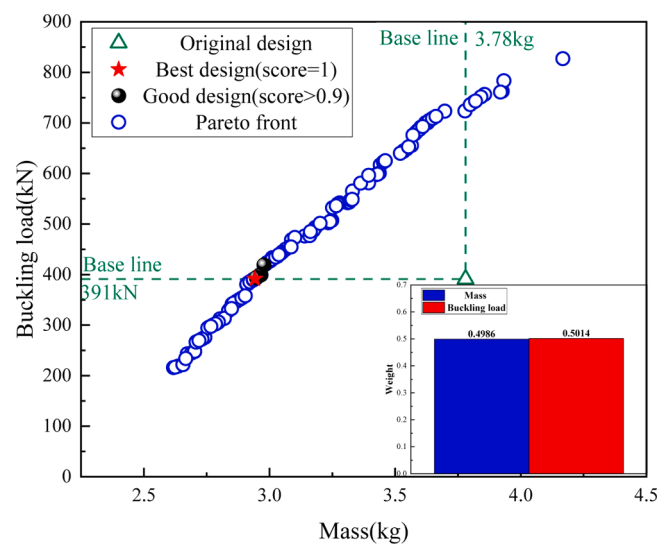


Fig. 12. Solving the Pareto front by TOPSIS method.

Table 4
Designs with top three scores.

	Score NO.1(score = 1)	Score NO.2(score = 0.988)	Score NO.3(score = 0.985)
θ_1	[45/0 ₂ /-45/90/ 45/0 ₃ /-45/0] _s	[45/0 ₂ /-45/90/ 45/0 ₃ /-45/0] _s	[45/0 ₂ /-45/90/ 45/0 ₃ /-45/0] _s
θ_2	[45/0 ₃ /-45 ₂ /90/ 45/0] _s	[45/0 ₃ /-45 ₂ /90/ 45/0] _s	[45/0 ₃ /-45 ₂ /90/ 45/0] _s
x_1	0.127 mm	0.127 mm	0.128 mm
x_2	0.130 mm	0.131 mm	0.129 mm
x_3	Material lab No.16	Material lab No.16	Material lab No.16
x_4	Material lab No.30	Material lab No.30	Material lab No.30
Reduction in Mass	22.18 %	22.02 %	22.00 %
Increase in P_b^e	0.11 %	0.58 %	0.83 %

design differences lie in the ply thickness of the skin and stiffeners. The design with the highest score features skin ply thickness of 0.127 mm and stiffener ply thickness of 0.130 mm, resulting in mass reduction of 22.18 % and buckling load increase of 0.11 % compared to the original design. The second-ranked design also has skin ply thickness of 0.127 mm, but stiffener ply thickness of 0.131 mm. This design achieves mass reduction of 22.02 % and buckling load increase of 0.58 % relative to the original design. Lastly, the third-ranked design has skin ply thickness of 0.128 mm and stiffener ply thickness of 0.129 mm, resulting in mass decrease of 22.00 % and buckling load increase of 0.83 % compared to the original design.

5. Conclusion

A novel multi-objective optimization framework for composite stiffened panels is proposed in this study, leveraging a combination of the Parallel Neural Network (PNN), Non-dominated Sorting Genetic Algorithm-III (NSGA-III), and Technique for Order Preference by Similarity to Ideal Solution (TOPSIS) method. Firstly, a refined surrogate model is meticulously constructed utilizing the PNN feature extraction method. Subsequently, the optimization problem is solved by NSGA-III algorithm, leading to the derivation of Pareto front. Lastly, the optimal design within the Pareto front is discerned employing the TOPSIS method. In general, the main advantages of our proposed method lie in three-phase:

1) The PNN model employed addresses the limitations of prior models, including non-independent input parameters, challenges in range determination, and the requirement for secondary solving. The approach presented in this article enables the establishment of the high-precision surrogate model through the data-driven method, eliminating the need for additional costs or deep understanding of physical laws, thereby enhancing cost efficiency and industrial applicability.

Appendix A. Material library

Material No.	Material parameters					
1 [78]	E_{11} 134.7 GPa	E_{22} ρ 1590 kg/m ³	G_{12} 4.2 GPa	G_{13} 4.2 GPa	G_{23} 2.5 GPa	
2 [79]	E_{11} 145 GPa	E_{22} ρ 1450 kg/m ³	G_{12} 5 GPa	G_{13} 5 GPa	G_{23} 3.5 GPa	
3 [80]	E_{11} 101.7 GPa	E_{22} ρ 1700 kg/m ³	G_{12} 2.4 GPa	G_{13} 2.4 GPa	G_{23} 2.4 GPa	

(continued on next page)

- 2) the proposed optimization method features an end-to-end structure, integrating proxy model construction, optimization calculations, and Pareto set solutions through automated and predefined methods. This minimizes human interference and significantly reduces the reliance on specialized knowledge.
- 3) Compared with the conventional optimization methods, our proposed method has a fast optimization speed, which only takes several minutes to fulfil the optimization process.

This article validates the proposed method's accuracy through multi-objective optimization aimed at maximizing buckling load and minimizing mass for composite stiffened panels. It evaluates the effectiveness of this method in terms of surrogate model accuracy, optimization results, and optimal design determination. The findings demonstrate significant practical application potential, offering guidance for operators involved in the optimization design of composite material structures in real-world scenarios. However, with the advent of Automatic Tape Laying (ATL) and Automated Fiber Placement (AFP) technologies, composite manufacturing is no longer limited to traditional stacking and straight fibers [76,77]. Future research will focus on optimizing the design of such advanced composite structures.

CRediT authorship contribution statement

Tao Zhang: Writing – review & editing, Writing – original draft, Supervision, Software, Methodology, Formal analysis, Data curation, Conceptualization. **Zhao Wei:** Writing – review & editing, Validation, Resources, Project administration, Funding acquisition, Conceptualization. **Liping Wang:** Writing – review & editing, Validation, Supervision, Project administration. **Zhuo Xue:** Writing – review & editing, Visualization, Validation, Supervision. **Suiyan Wang:** Writing – review & editing, Visualization, Validation, Supervision. **Peiyan Wang:** Writing – review & editing, Visualization, Validation, Supervision. **Bowen Qi:** Writing – review & editing, Visualization, Validation, Resources. **Zhufeng Yue:** Writing – review & editing, Validation, Supervision, Software.

Declaration of competing interest

The authors declare that they have no known competing financial interests or personal relationships that could have appeared to influence the work reported in this paper.

Acknowledgments

This investigation is supported by the National Natural Science Foundation of China, grant number [No. 12002399]. The authors would also like to deliver their sincere thanks to the editors and anonymous reviewers.

(continued)

Material No.	Material parameters				
	E_{11}	E_{22}	G_{12}	G_{13}	G_{23}
4 [81]	121 GPa	5.82 GPa	4 GPa	4 GPa	4 GPa
	ν_{12}	ρ			
	0.3	1580 kg/m ³			
5 [82]	126.1 GPa	11.2 GPa	5.46 GPa	5.46 GPa	5.46 GPa
	ν_{12}	ρ			
	0.3	1560 kg/m ³			
6 [82]	25 GPa	25 GPa	3 GPa	3 GPa	3 GPa
	ν_{12}	ρ			
	0.3	2200 kg/m ³			
7 [83]	131 GPa	8 GPa	4.5 GPa	4.5 GPa	3.5 GPa
	ν_{12}	ρ			
	0.29	1544 kg/m ³			
8 [84]	77.46 GPa	77.46 GPa	4.15 GPa	3.625 GPa	3.625 GPa
	ν_{12}	ρ			
	0.03	1655 kg/m ³			
9 [85]	155 GPa	12.1 GPa	4.4 GPa	4.4 GPa	3.2 GPa
	ν_{12}	ρ			
	0.248	1600 kg/m ³			
10 [86]	127.7 GPa	9.67 GPa	6.5 GPa	6.5 GPa	3.6 GPa
	ν_{12}	ρ			
	0.3	1520.7 kg/m ³			
11 [87]	131 GPa	13 GPa	6.41 GPa	6.41 GPa	6.41 GPa
	ν_{12}	ρ			
	0.38	1522 kg/m ³			
12 [88]	135 GPa	10 GPa	5 GPa	5 GPa	5 GPa
	ν_{12}	ρ			
	0.3	1600 kg/m ³			
13 [88]	45 GPa	10 GPa	5 GPa	5 GPa	5 GPa
	ν_{12}	ρ			
	0.3	2000 kg/m ³			
14 [89]	164 GPa	12.8 GPa	4.5 GPa	4.5 GPa	2.5 GPa
	ν_{12}	ρ			
	0.32	1800 kg/m ³			
15 [89]	38 GPa	8.27 GPa	4.14 GPa	4.14 GPa	4 GPa
	ν_{12}	ρ			
	0.25	1900 kg/m ³			
16 [89]	195 GPa	14.6 GPa	7.5 GPa	7.5 GPa	5 GPa
	ν_{12}	ρ			
	0.3	1400 kg/m ³			
17 [90]	161 GPa	9 GPa	6.1 GPa	6.1 GPa	6.1 GPa
	ν_{12}	ρ			
	0.26	1580 kg/m ³			
18 [91]	137.9 GPa	8.96 GPa	7.1 GPa	7.1 GPa	6.21 GPa
	ν_{12}	ρ			
	0.3	1600 kg/m ³			
19 [92]	145 GPa	10.3 GPa	5.3 GPa	5.275 GPa	3.95 GPa
	ν_{12}	ρ			
	0.301	1590 kg/m ³			
20 [93]	160 GPa	8.97 GPa	6.21 GPa	6.21 GPa	3.45 GPa
	ν_{12}	ρ			
	0.016	2700 kg/m ³			
21 [93]	80 GPa	80 GPa	6.48 GPa	5.1 GPa	4.07 GPa
	ν_{12}	ρ			
	0.06	1610 kg/m ³			
22 [94]	150.15 GPa	12.02 GPa	6.11 GPa	6.11 GPa	6.11 GPa
	ν_{12}	ρ			
	0.3	1790 kg/m ³			

(continued on next page)

(continued)

Material No.	Material parameters				
23 [95]	E_{11} 58.6 GPa ν_{12} 0.048	E_{22} 58.6 GPa ρ 1510 kg/m ³	G_{12} 3.06 GPa	G_{13} 3.06 GPa	G_{23} 3.06 GPa
24 [96]	E_{11} 136.5 GPa ν_{12} 0.27	E_{22} 10.1 GPa ρ 1530 kg/m ³	G_{12} 3.975 GPa	G_{13} 3.975 GPa	G_{23} 3.975 GPa
25 [96]	E_{11} 101 GPa ν_{12} 0.27	E_{22} 16.7 GPa ρ 1530 kg/m ³	G_{12} 3.4 GPa	G_{13} 3.4 GPa	G_{23} 3.4 GPa
26 [96]	E_{11} 103.8 GPa ν_{12} 0.28	E_{22} 6.55 GPa ρ 1530 kg/m ³	G_{12} 2.9 GPa	G_{13} 2.9 GPa	G_{23} 2.9 GPa
27 [97]	E_{11} 57.765 GPa ν_{12} 0.048	E_{22} 53.686 GPa ρ 1510 kg/m ³	G_{12} 3.065 GPa	G_{13} 3.065 GPa	G_{23} 3.065 GPa
28 [98]	E_{11} 119.6 GPa ν_{12} 0.27	E_{22} 9.2 GPa ρ 1800 kg/m ³	G_{12} 4 GPa	G_{13} 4 GPa	G_{23} 4 GPa
29 [99]	E_{11} 125 GPa ν_{12} 0.3	E_{22} 11.3 GPa ρ 1478 kg/m ³	G_{12} 5.43 GPa	G_{13} 5.43 GPa	G_{23} 3.979 GPa
30 [100]	E_{11} 210 GPa ν_{12} 0.3	E_{22} 45 GPa ρ 1500 kg/m ³	G_{12} 7.45 GPa	G_{13} 7.45 GPa	G_{23} 4 GPa
31 [101]	E_{11} 138 GPa ν_{12} 0.3	E_{22} 8.96 GPa ρ 1600 kg/m ³	G_{12} 7.1 GPa	G_{13} 7.1 GPa	G_{23} 6.2 GPa
32 [101]	E_{11} 131 GPa ν_{12} 0.22	E_{22} 10.3 GPa ρ 1500 kg/m ³	G_{12} 6.9 GPa	G_{13} 6.2 GPa	G_{23} 6.2 GPa
33 [101]	E_{11} 207 GPa ν_{12} 0.3	E_{22} 20.7 GPa ρ 2000 kg/m ³	G_{12} 6.9 GPa	G_{13} 6.9 GPa	G_{23} 4.1 GPa
34 [102]	E_{11} 155 GPa ν_{12} 0.3	E_{22} 8 GPa ρ 1600 kg/m ³	G_{12} 4 GPa	G_{13} 4 GPa	G_{23} 4 GPa
35 [103]	E_{11} 155 GPa ν_{12} 0.248	E_{22} 12.1 GPa ρ 1600 kg/m ³	G_{12} 4.4 GPa	G_{13} 4.4 GPa	G_{23} 3.2 GPa

Note: In this article, when both tensile and compressive stiffness are present, average stiffness values are calculated. If only G_{12} , default $G_{12} = G_{13} = G_{23}$.

Data availability

Data will be made available on request.

References

- [1] M.A. Bessa, S. Pellegrino, Design of ultra-thin shell structures in the stochastic post-buckling range using Bayesian machine learning and optimization, Int. J. Solids Struct. 139–140 (2018) 174–188, <https://doi.org/10.1016/j.ijsolstr.2018.01.035>.
- [2] M.-K. Kazi, F. Eljack, E. Mahdi, Data-driven modeling to predict the load vs. displacement curves of targeted composite materials for industry 4.0 and smart manufacturing, Compos. Struct. 258 (2021) 113207, <https://doi.org/10.1016/j.compstruct.2020.113207>.
- [3] U.K. Mallela, A. Upadhyay, Buckling of laminated composite stiffened panels subjected to in-plane shear: a parametric study, Thin-Walled Struct. 44 (2006) 354–361, <https://doi.org/10.1016/j.tws.2006.03.008>.
- [4] H. Ghiasi, D. Pasini, L. Lessard, Optimum stacking sequence design of composite materials part I: constant stiffness design, Compos. Struct. 90 (2009) 1–11, <https://doi.org/10.1016/j.composites.2009.01.006>.
- [5] H. Chagraoui, T. Lazghab, M. Soula, Buckling optimization and post-buckling analysis of omega sub-stiffened composite panels using different cohesive interface properties, Thin-Walled Struct. 189 (2023) 110944, <https://doi.org/10.1016/j.tws.2023.110944>.
- [6] F.-X. Irisarri, F. Laurin, F.-H. Leroy, J.-F. Maire, Computational strategy for multiobjective optimization of composite stiffened panels, Compos. Struct. 93 (2011) 1158–1167, <https://doi.org/10.1016/j.composites.2010.10.005>.
- [7] G. Soremekun, Z. Gürdal, C. Kassapoglou, D. Toni, Stacking sequence blending of multiple composite laminates using genetic algorithms, Compos. Struct. 56 (2002) 53–62, [https://doi.org/10.1016/S0263-8223\(01\)00185-4](https://doi.org/10.1016/S0263-8223(01)00185-4).
- [8] H.-T. Fan, H. Wang, X.-H. Chen, An optimization method for composite structures with ply-drops, Compos. Struct. 136 (2016) 650–661, <https://doi.org/10.1016/j.composites.2015.11.003>.
- [9] A.A. Vijayachandran, P. Davidson, A.M. Waas, Optimal fiber paths for robotically manufactured composite structural panels, Int. J. Non Linear Mech. 126 (2020) 103567, <https://doi.org/10.1016/j.ijnonlinmec.2020.103567>.

- [10] M. Rouhi, H. Ghayoor, S.V. Hoa, M. Hojjati, Multi-objective design optimization of variable stiffness composite cylinders, *Compos. Part B: Eng.* 69 (2015) 249–255, <https://doi.org/10.1016/j.compositesb.2014.10.011>.
- [11] R. Butler, F.W. Williams, Optimum design using viconopt, a buckling and strength constraint program for prismatic assemblies of anisotropic plates, *Comput. Struct.* 43 (1992) 699–708, [https://doi.org/10.1016/0045-7949\(92\)90511-W](https://doi.org/10.1016/0045-7949(92)90511-W).
- [12] X. Liu, C.A. Featherston, D. Kennedy, Two-level layup optimization of composite laminate using lamination parameters, *Compos. Struct.* 211 (2019) 337–350, <https://doi.org/10.1016/j.compstruct.2018.12.054>.
- [13] X. Liu, C.A. Featherston, D. Kennedy, Buckling optimization of blended composite structures using lamination parameters, *Thin-Walled Struct.* 154 (2020) 106861, <https://doi.org/10.1016/j.tws.2020.106861>.
- [14] T. Le-Manh, J. Lee, Stacking sequence optimization for maximum strengths of laminated composite plates using genetic algorithm and isogeometric analysis, *Compos. Struct.* 116 (2014) 357–363, <https://doi.org/10.1016/j.compstruct.2014.05.011>.
- [15] P. Malekzadeh, A.R. Vosoughi, DQM large amplitude vibration of composite beams on nonlinear elastic foundations with restrained edges, *Commun. Nonlinear Sci. Numer. Simul.* 14 (2009) 906–915, <https://doi.org/10.1016/j.cnsns.2007.10.014>.
- [16] M.H. Sadri, H.Ghashchi Bargh, Optimization of laminated composite plates for maximum fundamental frequency using Elitist-Genetic algorithm and finite strip method, *J. Glob. Optim.* 54 (2012) 707–728, <https://doi.org/10.1007/s10898-011-9787-x>.
- [17] R. Rikards, H. Abramovich, J. Auzins, A. Korjakins, O. Ozolinsh, K. Kalnins, T. Green, Surrogate models for optimum design of stiffened composite shells, *Compos. Struct.* 63 (2004) 243–251, [https://doi.org/10.1016/S0263-8223\(03\)00171-5](https://doi.org/10.1016/S0263-8223(03)00171-5).
- [18] A.A. Vijayachandran, A.M. Waas, Minimizing stress concentrations using steered fiberpaths and incorporating realistic manufacturing signatures, *Int. J. Non Linear Mech.* 146 (2022) 104160, <https://doi.org/10.1016/j.ijnonlinmec.2022.104160>.
- [19] Q. Guo, J. Hang, S. Wang, W. Hui, Z. Xie, Buckling optimization of variable stiffness composite cylinders by using multi-fidelity surrogate models, *Thin-Walled Struct.* 156 (2020) 107014, <https://doi.org/10.1016/j.tws.2020.107014>.
- [20] S. Sikdar, W. Ostachowicz, A. Kundu, Deep learning for automatic assessment of breathing-debonds in stiffened composite panels using non-linear guided wave signals, *Compos. Struct.* 312 (2023) 116876, <https://doi.org/10.1016/j.compstruct.2023.116876>.
- [21] Y. Liu, Z. Lei, R. Zhu, Y. Shang, R. Bai, Artificial neural network prediction of residual compressive strength of composite stiffened panels with open crack, *Ocean Eng.* 266 (2022) 112771, <https://doi.org/10.1016/j.oceaneng.2022.112771>.
- [22] U.K. Mallela, A. Upadhyay, Buckling load prediction of laminated composite stiffened panels subjected to in-plane shear using artificial neural networks, *Thin-Walled Struct.* 102 (2016) 158–164, <https://doi.org/10.1016/j.tws.2016.01.025>.
- [23] Z. Sun, Z. Lei, R. Bai, H. Jiang, J. Zou, Y. Ma, C. Yan, Prediction of compression buckling load and buckling mode of hat-stiffened panels using artificial neural network, *Eng. Struct.* 242 (2021) 112275, <https://doi.org/10.1016/j.engstruct.2021.112275>.
- [24] Z. Sun, Z. Lei, J. Zou, R. Bai, H. Jiang, C. Yan, Prediction of failure behavior of composite hat-stiffened panels under in-plane shear using artificial neural network, *Compos. Struct.* 272 (2021) 114238, <https://doi.org/10.1016/j.compstruct.2021.114238>.
- [25] Optimization of variable-stiffness panels for maximum buckling load using lamination parameters, (n.d.). <https://doi.org/10.2514/1.42490>.
- [26] Buckling response of laminates with spatially varying fiber orientations, (n.d.). <https://arc.aiaa.org/doi/epdf/10.2514/6.1993-1567> (accessed August 29, 2024).
- [27] Chuquai et al., 2021. A data-driven Bayesian optimisation framework for the design and stacking.pdf, (n.d.). <https://www.sciencedirect.com/science/article/pii/S1359836821007186/pdf?md5=6947900a8a547829f708551beb5e53b&pid=1-s2.0-S1359836821007186-main.pdf&isDTMRedir=Y> (accessed July 23, 2023).
- [28] H. Fukunaga, G.N. Vanderplaats, Stiffness optimization of orthotropic laminated composites using lamination parameters, *AIAA J.* 29 (1991) 641–646, <https://doi.org/10.2514/3.59931>.
- [29] J.L. Grenestedt, P. Gudmundson, Layup optimization of composite material structures, in: P. Pedersen (Ed.), *Optimal Design with Advanced Materials*, Elsevier, Oxford, 1993, pp. 311–336, <https://doi.org/10.1016/B978-0-444-89869-2.50027-5>.
- [30] V.B. Hammer, M.P. Bendsøe, R. Lipton, P. Pedersen, Parametrization in laminate design for optimal compliance, *Int. J. Solids Struct.* 34 (1997) 415–434, [https://doi.org/10.1016/S0020-7683\(96\)00023-6](https://doi.org/10.1016/S0020-7683(96)00023-6).
- [31] T. Zhang, P. Wang, J. Fu, S. Wang, C. Lian, Parallel neural network feature extraction method for predicting buckling load of composite stiffened panels, *Thin-Walled Struct.* (2024) 111797, <https://doi.org/10.1016/j.tws.2024.111797>.
- [32] Concurrent stacking sequence and layout optimization of stiffened composite plates using a spectral element method and an index-based optimization technique, *Compos. Struct.* 327 (2024) 117698, <https://doi.org/10.1016/j.compstruct.2023.117698>.
- [33] H. Chagraoui, T. Lazghab, M. Soula, Buckling optimization and post-buckling analysis of omega sub-stiffened composite panels using different cohesive interface properties, *Thin-Walled Struct.* 189 (2023) 110944, <https://doi.org/10.1016/j.tws.2023.110944>.
- [34] S. Moradi, A.R. Vosoughi, N. Anjabin, Maximum buckling load of stiffened laminated composite panel by an improved hybrid PSO-GA optimization technique, *Thin-Walled Struct.* 160 (2021) 107382, <https://doi.org/10.1016/j.tws.2020.107382>.
- [35] X. Liu, J. Qin, K. Zhao, C.A. Featherston, D. Kennedy, Y. Jing, G. Yang, Design optimization of laminated composite structures using artificial neural network and genetic algorithm, *Compos. Struct.* 305 (2023) 116500, <https://doi.org/10.1016/j.compstruct.2022.116500>.
- [36] L. Marín, D. Trias, P. Badalló, G. Rus, J.A. Mayugo, Optimization of composite stiffened panels under mechanical and hydrothermal loads using neural networks and genetic algorithms, *Compos. Struct.* 94 (2012) 3321–3326, <https://doi.org/10.1016/j.compstruct.2012.04.024>.
- [37] R. Susmaga, I. Szczęch, D. Brzezinski, Towards explainable TOPSIS: visual insights into the effects of weights and aggregations on rankings, *Appl. Soft Comput.* 153 (2024) 111279, <https://doi.org/10.1016/j.asoc.2024.111279>.
- [38] Z. Gürdal, R.T. Haftka, P. Hajela, *Design and Optimization of Laminated Composite Materials*, John Wiley & Sons, 1999.
- [39] H. Liu, Z. Zhang, H. Jia, Q. Li, Y. Liu, J. Leng, A novel method to predict the stiffness evolution of in-service wind turbine blades based on deep learning models, *Compos. Struct.* 252 (2020) 112702, <https://doi.org/10.1016/j.compstruct.2020.112702>.
- [40] Q. Chen, R. Jia, S. Pang, Deep long short-term memory neural network for accelerated elastoplastic analysis of heterogeneous materials: an integrated data-driven surrogate approach, *Compos. Struct.* 264 (2021) 113688, <https://doi.org/10.1016/j.compstruct.2021.113688>.
- [41] Z. Niu, G. Zhong, H. Yu, A review on the attention mechanism of deep learning, *Neurocomputing* 452 (2021) 48–62, <https://doi.org/10.1016/j.neucom.2021.03.091>.
- [42] G. Brauwers, F. Frasincar, A general survey on attention mechanisms in deep learning, *IEEE Trans. Knowl. Data Eng.* 35 (2023) 3279–3298, <https://doi.org/10.1109/TKDE.2021.3126456>.
- [43] S. Chaudhari, V. Mithal, G. Polatkan, R. Ramanath, An attentive survey of attention models, *arXiv.Org* (2019). <https://arxiv.org/abs/1904.02874v3> (accessed October 13, 2023).
- [44] S. Hochreiter, J. Schmidhuber, Long Short-Term Memory, *Neural Comput.* 9 (1997) 1735–1780, <https://doi.org/10.1162/neco.1997.9.8.1735>.
- [45] A. Vaswani, N. Shazeer, N. Parmar, J. Uszkoreit, L. Jones, A.N. Gomez, L. Kaiser, I. Polosukhin, Attention is all you need, *arXiv.Org* (2017). <https://arxiv.org/abs/1706.03762v7> (accessed October 13, 2023).
- [46] T. Mikolov, K. Chen, G. Corrado, J. Dean, Efficient estimation of word representations in vector space, *arXiv.Org* (2013). <https://arxiv.org/abs/1301.3781v3> (accessed October 13, 2023).
- [47] K. He, X. Zhang, S. Ren, J. Sun, Deep residual learning for image recognition, in: 2016 IEEE Conference on Computer Vision and Pattern Recognition (CVPR), Las Vegas, NV, USA, IEEE, 2016, pp. 770–778, <https://doi.org/10.1109/CVPR.2016.90>.
- [48] J.L. Ba, J.R. Kiros, G.E. Hinton, Layer normalization, *arXiv.Org* (2016). <https://arxiv.org/abs/1607.06450v1> (accessed October 13, 2023).
- [49] M. Lin, Q. Chen, S. Yan, Network in network, *arXiv.Org* (2013). <https://arxiv.org/abs/1312.4400v3> (accessed October 13, 2023).
- [50] G. Klambauer, T. Unterthiner, A. Mayr, S. Hochreiter, Self-normalizing neural networks, *arXiv.Org* (2017). <https://arxiv.org/abs/1706.02515v5> (accessed October 13, 2023).
- [51] D.P. Kingma, J. Lei, Adam: a method for stochastic optimization, (2015).
- [52] T. Akiba, S. Sano, T. Yanase, T. Ohta, M. Koyama, Optuna: a next-generation hyperparameter optimization framework, in: Proceedings of the 25th ACM SIGKDD International Conference on Knowledge Discovery & Data Mining, New York, NY, USA, Association for Computing Machinery, 2019, pp. 2623–2631, <https://doi.org/10.1145/3292500.3330701>.
- [53] D. Ma, S. Zhou, Y. Han, W. Ma, H. Huang, Multi-objective ship weather routing method based on the improved NSGA-III algorithm, *J. Ind. Inf. Integr.* 38 (2024) 100570, <https://doi.org/10.1016/j.jii.2024.100570>.
- [54] J.-H. Yi, S. Deb, J. Dong, A.H. Alavi, G.-G. Wang, An improved NSGA-III algorithm with adaptive mutation operator for big data optimization problems, *Future Gen. Comput. Syst.* 88 (2018) 571–585, <https://doi.org/10.1016/j.future.2018.06.008>.
- [55] K. Deb, H. Jain, An evolutionary many-objective optimization algorithm using reference-point-based nondominated sorting approach, part I: solving problems with box constraints, *IEEE Trans. Evol. Comput.* 18 (2014) 577–601, <https://doi.org/10.1109/TEVC.2013.2281535>.
- [56] T. Vo-Duy, D. Duong-Gia, V. Ho-Huu, H.C. Vu-Do, T. Nguyen-Thoi, Multi-objective optimization of laminated composite beam structures using NSGA-II algorithm, *Compos. Struct.* 168 (2017) 498–509, <https://doi.org/10.1016/j.compstruct.2017.02.038>.
- [57] K. Deb, A. Pratap, S. Agarwal, T. Meyarivan, A fast and elitist multiobjective genetic algorithm: NSGA-II, *IEEE Trans. Evol. Comput.* 6 (2002) 182–197, <https://doi.org/10.1109/4235.996017>.
- [58] J. Zhang, S. Wang, Q. Tang, Y. Zhou, T. Zeng, An improved NSGA-III integrating adaptive elimination strategy to solution of many-objective optimal power flow problems, *Energy* 172 (2019) 945–957, <https://doi.org/10.1016/j.energy.2019.02.009>.
- [59] Z.-M. Gu, G.-W. Wang, Improving NSGA-III algorithms with information feedback models for large-scale many-objective optimization, *Future Gen. Comput. Syst.* 107 (2020) 49–69, <https://doi.org/10.1016/j.future.2020.01.048>.
- [60] M. Montemurro, A. Vincenti, P. Vannucci, Design of the elastic properties of laminates with a minimum number of plies, *Mech. Compos. Mater.* 48 (2012) 369–390, <https://doi.org/10.1007/s11029-012-9284-4>.

- [61] M. Montemurro, Y. Koutsawa, S. Belouettar, A. Vincenti, P. Vannucci, Design of damping properties of hybrid laminates through a global optimisation strategy, *Compos. Struct.* 94 (2012) 3309–3320, <https://doi.org/10.1016/j.compstruct.2012.05.003>.
- [62] R. Le Riche, R.T. Haftka, Improved genetic algorithm for minimum thickness composite laminate design, *Compos. Eng.* 5 (1995) 143–161, [https://doi.org/10.1016/0961-9526\(95\)90710-S](https://doi.org/10.1016/0961-9526(95)90710-S).
- [63] N. Fedon, P.M. Weaver, A. Pirrera, T. Macquart, A repair algorithm for composite laminates to satisfy lay-up design guidelines, *Compos. Struct.* 259 (2021) 113448, <https://doi.org/10.1016/j.compstruct.2020.113448>.
- [64] M. Abdel-Basset, R. Mohamed, M. Abouhawwash, A.M. Alshamrani, A. Wagdy Mohamed, K. Sallam, Binary light spectrum optimizer for knapsack problems: an improved model, *Alex. Eng. J.* 67 (2023) 609–632, <https://doi.org/10.1016/j.aej.2022.12.025>.
- [65] Simulated binary crossover for continuous search space by kalyanmoy deb and ram bhushan agrawal, (n.d.). https://www.complex-systems.com/abstracts/v09_i02_a02/ (accessed March 1, 2024).
- [66] K. Deb, K. Sindhya, T. Okabe, Self-adaptive simulated binary crossover for real-parameter optimization, in: Proceedings of the 9th Annual Conference on Genetic and Evolutionary Computation, New York, NY, USA, Association for Computing Machinery, 2007, pp. 1187–1194, <https://doi.org/10.1145/1276958.1277190>.
- [67] S. Bandaru, R. Tulshyan, K. Deb, Modified SBX and adaptive mutation for real world single objective optimization, in: 2011: pp. 1335–1342. <https://doi.org/10.1109/CEC.2011.5949771>.
- [68] G.-Q. Zeng, J. Chen, L.-M. Li, M.-R. Chen, L. Wu, Y.-X. Dai, C.-W. Zheng, An improved multi-objective population-based extremal optimization algorithm with polynomial mutation, *Inf. Sci. (Ny)* 330 (2016) 49–73, <https://doi.org/10.1016/j.ins.2015.10.010>.
- [69] P.-H. Tang, M.-H. Tseng, Adaptive directed mutation for real-coded genetic algorithms, *Appl. Soft Comput. J.* 13 (2013) 600–614, <https://doi.org/10.1016/j.asoc.2012.08.035>.
- [70] H. Jain, K. Deb, An evolutionary many-objective optimization algorithm using reference-point based nondominated sorting approach, part II: handling constraints and extending to an adaptive approach, *IEEE Trans. Evol. Comput.* 18 (2014) 602–622, <https://doi.org/10.1109/TEVC.2013.2281534>.
- [71] E. Bottani, A. Rizzi, A fuzzy TOPSIS methodology to support outsourcing of logistics services, *Supply Chain Manage.* 11 (2006) 294–308, <https://doi.org/10.1108/13598540610671743>.
- [72] W.-P. Wang, Toward developing agility evaluation of mass customization systems using 2-tuple linguistic computing, *Expert Syst. Appl.* 36 (2009) 3439–3447, <https://doi.org/10.1016/j.eswa.2008.02.015>.
- [73] Z. Zhang, H. Jiang, T. Shao, Q. Shao, Understanding the selection of intelligent engineering B2B platform in China through the fuzzy DANP and TOPSIS techniques: a multi-study analysis, *Appl. Soft Comput.* 141 (2023), <https://doi.org/10.1016/j.asoc.2023.110277>.
- [74] X. Yu, S. Guo, J. Guo, X. Huang, Rank B2C e-commerce websites in e-alliance based on AHP and fuzzy TOPSIS, *Expert Syst. Appl.* 38 (2011) 3550–3557, <https://doi.org/10.1016/j.eswa.2010.08.143>.
- [75] S.-S. Lin, A. Zhou, S.-L. Shen, Safety assessment of excavation system via TOPSIS-based MCDM modelling in fuzzy environment, *Appl. Soft Comput.* 138 (2023), <https://doi.org/10.1016/j.asoc.2023.110206>.
- [76] A.W. Blom, M.M. Abdalla, Z. Gürdal, Optimization of course locations in fiber-placed panels for general fiber angle distributions, *Compos. Sci. Technol.* 70 (2010) 564–570, <https://doi.org/10.1016/j.compscitech.2009.12.003>.
- [77] M. Arian Nik, K. Fayazbakhsh, D. Pasini, L. Lessard, Optimization of variable stiffness composites with embedded defects induced by automated fiber placement, *Compos. Struct.* 107 (2014) 160–166, <https://doi.org/10.1016/j.compstruct.2013.07.059>.
- [78] K. Asakawa, Y. Hirano, K.-T. Tan, T. Ogasawara, Bio-inspired study of stiffener arrangement in composite stiffened panels using a Voronoi diagram as an indicator, *Compos. Struct.* 327 (2024) 117640, <https://doi.org/10.1016/j.compstruct.2023.117640>.
- [79] B.G. Falzon, K.A. Stevens, G.O. Davies, Postbuckling behaviour of a blade-stiffened composite panel loaded in uniaxial compression, *Compos. Part A: Appl. Sci. Manuf.* 31 (2000) 459–468, [https://doi.org/10.1016/S1359-835X\(99\)00085-8](https://doi.org/10.1016/S1359-835X(99)00085-8).
- [80] X. Lian, W. Zhang, Y. Mao, Z. Yu, Buckling optimization of curved grid-stiffened helicoidal composite panel including the factor of mode shape in multiple load cases, *Compos. Struct.* 322 (2023) 117383, <https://doi.org/10.1016/j.compstruct.2023.117383>.
- [81] M. Liu, Y. Gao, D. Zhang, Z. Wang, D. Wu, B. Yu, Y. Lei, An enhanced elastoplastic damage coupled model for compression characteristics analysis of continuous fiber-reinforced thermoplastic composite stiffened panel, *Compos. Struct.* 297 (2022) 115924, <https://doi.org/10.1016/j.compstruct.2022.115924>.
- [82] K.S. van Dooren, B.H.A.H. Tijs, J.E.A. Waleson, C. Bisagni, Skin-stringer separation in post-buckling of butt-joint stiffened thermoplastic composite panels, *Compos. Struct.* 304 (2023) 116294, <https://doi.org/10.1016/j.compstruct.2022.116294>.
- [83] B. da Silva Henriques, P. Ribeiro, M.F.S.F. de Moura, R. Pullin, Non-linear dynamics of a stiffened composite laminated panel with debonds, *Compos. Struct.* 321 (2023) 117233, <https://doi.org/10.1016/j.compstruct.2023.117233>.
- [84] S. Sikdar, W. Ostachowicz, A. Kundu, Deep learning for automatic assessment of breathing-debonds in stiffened composite panels using non-linear guided wave signals, *Compos. Struct.* 312 (2023) 116876, <https://doi.org/10.1016/j.compstruct.2023.116876>.
- [85] A. Alhajahmad, C. Mittelstedt, Minimum weight design of curvilinearly grid-stiffened variable-stiffness composite fuselage panels considering buckling and manufacturing constraints, *Thin-Walled Struct.* 161 (2021) 107526, <https://doi.org/10.1016/j.tws.2021.107526>.
- [86] K. Zheng, Z. Li, Z. Ma, J. Chen, J. Zhou, X. Su, Damage detection method based on Lamb waves for stiffened composite panels, *Compos. Struct.* 225 (2019) 111137, <https://doi.org/10.1016/j.compstruct.2019.111137>.
- [87] U.K. Mallela, A. Upadhyay, Buckling load prediction of laminated composite stiffened panels subjected to in-plane shear using artificial neural networks, *Thin-Walled Struct.* 102 (2016) 158–164, <https://doi.org/10.1016/j.tws.2016.01.025>.
- [88] E.S. Elumalai, G. Krishnaveni, R. Sarath Kumar, D. Dominic Xavier, G. Kavitha, S. Seralathan, V. Hariram, T. Micha Premkumar, Buckling analysis of stiffened composite curved panels, *Mater. Today Proc.* 33 (2020) 3604–3611, <https://doi.org/10.1016/j.mtproc.2020.05.662>.
- [89] Y.B. SudhirSastry, P.R. Budarapu, N. Madhavi, Y. Krishna, Buckling analysis of thin wall stiffened composite panels, *Comput. Mater. Sci.* 96 (2015) 459–471, <https://doi.org/10.1016/j.commatsci.2014.06.007>.
- [90] M. Montemurro, A. Pagani, G.A. Fiordilino, J. Pailhès, E. Carrera, A general multi-scale two-level optimisation strategy for designing composite stiffened panels, *Compos. Struct.* 201 (2018) 968–979, <https://doi.org/10.1016/j.compstruct.2018.06.119>.
- [91] H. Sekine, S. Atobe, Identification of locations and force histories of multiple point impacts on composite isogrid-stiffened panels, *Compos. Struct.* 89 (2009) 1–7, <https://doi.org/10.1016/j.compstruct.2008.05.018>.
- [92] A. Faggiani, B.G. Falzon, Predicting low-velocity impact damage on a stiffened composite panel, *Compos. Part A Appl. Sci. Manuf.* 41 (2010) 737–749, <https://doi.org/10.1016/j.compositesa.2010.02.005>.
- [93] Z. Song, J. Le, D. Whisler, H. Kim, Skin-stringer interface failure investigation of stringer-stiffened curved composite panels under hail ice impact, *Int. J. Impact Eng.* 122 (2018) 439–450, <https://doi.org/10.1016/j.ijimpeng.2018.09.014>.
- [94] H. Less, H. Abramovich, Dynamic buckling of a laminated composite stringer-stiffened cylindrical panel, *Compos. Part B Eng.* 43 (2012) 2348–2358, <https://doi.org/10.1016/j.compositesb.2011.11.070>.
- [95] C. Bisagni, L. Lanzi, Post-buckling optimisation of composite stiffened panels using neural networks, *Compos. Struct.* 58 (2002) 237–247, [https://doi.org/10.1016/S0263-8223\(02\)00053-3](https://doi.org/10.1016/S0263-8223(02)00053-3).
- [96] M. Corvino, L. Iuspa, A. Riccio, F. Scaramuzzino, Weight and cost oriented multi-objective optimisation of impact damage resistant stiffened composite panels, *Comput. Struct.* 87 (2009) 1033–1042, <https://doi.org/10.1016/j.compstruc.2008.04.020>.
- [97] L. Lanzi, A numerical and experimental investigation on composite stiffened panels into post-buckling, *Thin-Walled Struct.* 42 (2004) 1645–1664, <https://doi.org/10.1016/j.tws.2004.06.001>.
- [98] W. Bao, M. Li, X. An, H. Han, Y. Lou, H. Fan, Hierarchical-level failure analysis for CFRP lattice stiffened panel, *Thin-Walled Struct.* 183 (2023) 110354, <https://doi.org/10.1016/j.tws.2022.110354>.
- [99] C. Hu, Z. Xu, J. Qiu, S. Wu, R. Wang, X. He, A unified modeling strategy of the stability and progressive damage behavior of CFRP double-blade composite stiffened structures (DCSS) under uniaxial compression, *Thin-Walled Struct.* 189 (2023) 110896, <https://doi.org/10.1016/j.tws.2023.110896>.
- [100] L. Xiaoquan, Z. Yifeng, S. Zheng, C. Jiaqi, Forced vibration analysis of isogrid-stiffened composite plates using VAM-based equivalent plate model, *J. Sound Vib.* 541 (2022) 117314, <https://doi.org/10.1016/j.jsv.2022.117314>.
- [101] T. Fu, Z. Chen, D. Yu, X. Wang, W. Lu, Sound transmission from stiffened double laminated composite plates, *Wave Motion*. 72 (2017) 331–341, <https://doi.org/10.1016/j.wavemoti.2017.04.007>.
- [102] X. Wu, Q. Chen, B. Zhao, K. Zhang, P. Wang, Z. Yue, Experimental behavior and shear bearing capacity simulation of stiffened composite panels subjected to invisible damage impact, *Thin-Walled Struct.* 178 (2022) 109454, <https://doi.org/10.1016/j.tws.2022.109454>.
- [103] A. Alhajahmad, C. Mittelstedt, Buckling capacity of composite panels with cutouts using continuous curvilinear fibres and stiffeners based on streamlines, *Compos. Struct.* 281 (2022) 114974, <https://doi.org/10.1016/j.compstruct.2021.114974>.